

**BULETINUL
INSTITUTULUI
POLITEHNIC
DIN IAȘI**

**Volumul 63 (67)
Numărul 3**

**Secția
MATEMATICĂ
MECANICĂ TEORETICĂ
FIZICĂ**

2017

Editura POLITEHNIUM

BULETINUL INSTITUTULUI POLITEHNIC DIN IAȘI
PUBLISHED BY
“GHEORGHE ASACHI” TECHNICAL UNIVERSITY OF IAȘI
Editorial Office: Bd. D. Mangeron 63, 700050, Iași, ROMANIA
Tel. 40-232-278683; Fax: 40-232-237666; e-mail: polytech@mail.tuiasi.ro

Editorial Board

President: **Dan Cașcaval**,
Rector of the “Gheorghe Asachi” Technical University of Iași
Editor-in-Chief: **Maria Carmen Loghin**,
Vice-Rector of the “Gheorghe Asachi” Technical University of Iași
Honorary Editors of the Bulletin: **Alfred Braier**,
Mihail Voicu, Corresponding Member of the Romanian Academy,
Carmen Teodosiu

Editors in Chief of the **MATHEMATICS. THEORETICAL MECHANICS.**
PHYSICS Section

Maricel Agop, Narcisa Apreutesei-Dumitriu,
Daniel Condurache

Honorary Editors: **Cătălin Gabriel Dumitraș**

Associated Editor: **Petru Edward Nica**

Scientific Board

Sergiu Aizicovici, University “Ohio”, U.S.A.
Constantin Băcuță, University “Delaware”, Newark,
Delaware, U.S.A.

Masud Caichian, University of Helsinki, Finland

Adrian Cordunenu, “Gheorghe Asachi” Technical
University of Iași

Constantin Corduneanu, University of Texas,
Arlington, USA.

Piergiulio Corsini, University of Udine, Italy

Sever Dragomir, University “Victoria”, of Melbourne,
Australia

Constantin Fetecău, “Gheorghe Asachi” Technical
University of Iași

Cristi Foça, University of Lille, France

Tasawar Hayat, University “Quaid-i-Azam” of
Islamabad, Pakistan

Radu Ibănescu, “Gheorghe Asachi” Technical
University of Iași

Bogdan Kazmierczak, Inst. of Fundamental Research,
Warsaw, Poland

Liviu Leontie, “Al. I. Cuza” University, Iași
Rodica Luca-Tudorache, “Gheorghe Asachi”
Technical University of Iași

Radu Miron, “Al. I. Cuza” University of Iași
Iuliana Oprea, Colorado State University, U.S.A
Viorel-Puiu Păun, University “Politehnica” of
București

Lucia Pletea, “Gheorghe Asachi” Technical
University of Iași

Irina Radinschi, “Gheorghe Asachi” Technical
University of Iași

Themistocles Rassias, University of Athens, Greece

Behzad Djafari Rouhani, University of Texas at El
Paso, USA

Cristina Stan, University “Politehnica” of București
Wenchang Tan, University “Peking” Beijing, China

Petre P. Teodorescu, University of București

Anca Tureanu, University of Helsinki, Finland

Vitaly Volpert, CNRS, University “Claude Bernard”,
Lyon, France

Secția

MATEMATICĂ. MECANICĂ TEORETICĂ. FIZICĂ

S U M A R

	<u>Pag.</u>
IRINEL CASIAN BOTEZ, Generalizarea operatorului Nabla într-un spațiu unidimensional fracțional (engl., rez. rom.)	9
IRINEL CASIAN BOTEZ și MARICEL AGOP, Entanglement fraternal (engl., rez. rom.)	13
BIANCA CRISTIANA HODOROABĂ, Aspecte fundamentale ale ablației laser în lichid: Metoda ecologică de producere a nanoparticulelor (engl., rez. rom.)	23
CAMIL CIPRIAN MIREȘTEAN, CĂLIN GHEORGHE BUZEA și DRAGOȘ TEODOR IANCU, Considerații radiobiologice asupra tehnicilor moderne de radioterapie externă IMRT și VMAT (engl., rez. rom.)	33
CĂLIN GHEORGHE BUZEA, CAMIL CIPRIAN MIREȘTEAN și DRAGOȘ TEODOR IANCU, O aplicație pe calculator pentru predicția riscului de disfagie în radioterapia cancerului capului și gâtului (engl., rez. rom.)	39
OVIDIU NICOLAE PĂGUȚE, CAMIL CIPRIAN MIREȘTEAN, CĂLIN GHEORGHE BUZEA, RALUCA APOSTU, SIMONA CÎRDEI, TUDOR CIOBANU, COSMIN SAFTA și DRAGOȘ TEODOR IANCU, Comparatie dozimetrică între tehnicile IMRT și 3D-CRT în radioterapia posturgicală a liposarcomului pleomorf de coapsă (engl., rez. rom.)	45
IUSTINA HĂTESCU, CĂLIN GHEORGHE BUZEA, CĂTĂLIN BORCIA și DRAGOȘ TEODOR IANCU, Influența modelelor radiobiologice în evaluarea unui plan de tratament privind riscul de toxicitate a structurilor neurale la un pacient cu glioblastom tratat cu radioterapie (engl., rez. rom.)	53

Section

MATHEMATICS. THEORETICAL MECHANICS. PHYSICS

CONTENTS

	<u>Pp.</u>
IRINEL CASIAN BOTEZ, Generalization of Nabla Operator in Fractional One Dimensional Space (English, Romanian summary)	9
IRINEL CASIAN BOTEZ and MARICEL AGOP, Fractal Entanglement (English, Romanian summary)	13
BIANCA CRISTIANA HODOROABĂ, Fundamental Aspects of Laser Ablation in Liquid: Green Method for Nanoparticle Production (English, Romanian summary)	23
CAMIL CIPRIAN MIREȘTEAN, CĂLIN GHEORGHE BUZEA and DRAGOȘ TEODOR IANCU, Radiobiological Considerations on Modern Techniques of External Radiotherapy IMRT and VMAT (English, Romanian summary)	33
CĂLIN GHEORGHE BUZEA, CAMIL CIPRIAN MIREȘTEAN and DRAGOȘ TEODOR IANCU, A Computer Application for the Prediction of Risk of Dysphagia in the Irradiation of Head and Neck Cancer (English, Romanian summary)	39
OVIDIU NICOLAE PĂGUȚE, CAMIL CIPRIAN MIREȘTEAN, CĂLIN GHEORGHE BUZEA, RALUCA APOSTU, SIMONA CÎRDEI, TUDOR CIOBANU, COSMIN SAFTA and DRAGOȘ TEODOR IANCU, Dosimetric Comparison Between IMRT and 3D-CRT Techniques in Postsurgical Radiotherapy of a Pleomorf Liposarcoma of the Thigh (English, Romanian summary)	45
IUSTINA HĂTESCU, CĂLIN GHEORGHE BUZEA, CĂTĂLIN BORCIA and DRAGOȘ TEODOR IANCU, The Influence of Radiobiological Models in Evaluation of a Treatment Plan Regarding the Risk of Toxicity of Neural Structures in a Patient with Glioblastoma Treated with Radiotherapy (English, Romanian summary)	53

BULETINUL INSTITUTULUI POLITEHNIC DIN IAȘI
Publicat de
Universitatea Tehnică „Gheorghe Asachi” din Iași
Volumul 63 (67), Numărul 3, 2017
Secția
MATEMATICĂ. MECANICĂ TEORETICĂ. FIZICĂ

GENERALIZATION OF NABLA OPERATOR IN FRACTIONAL ONE DIMENSIONAL SPACE

BY

IRINEL CASIAN BOTEZ*

“Gheorghe Asachi” Technical University of Iași,
Faculty of Electronics, Telecommunication and Information Technology

Received: September 8, 2017

Accepted for publication: October 26, 2017

Abstract. Nabla operator in fractional one dimensional space have to be used for modeling the various dissipative systems, as the application in this paper proves.

Keywords: Fractional dimensional space; Nabla operator; dissipative systems.

1. Introduction

The non-integer dimension (D) occurs in certain key quantities such as Gaussian integral:

$$\int e^{-\alpha r^2} d\mathbf{r} = \left(\frac{\pi}{\alpha}\right)^{D/2}$$

Or the radial Laplace operator

$$\frac{\partial^2}{\partial r^2} + \frac{(D-1)}{r} \frac{\partial}{\partial r}$$

*Corresponding author; *e-mail*: irinel_casian@yahoo.com

This paper presents a mathematically concrete realisation of spaces with non-integer D .

2. Nabla Operator in Fractional Space

In the 1970s, (Stillinger, 1977) generalized the Laplace operator in a fractional space of dimension D , where D is a non-integer number:

$$\nabla_D^2 f(r) = f''(r) + \frac{D-1}{r} f'(r), \quad 0 < D \leq 1 \quad (1)$$

This confirm the compatibility of expressions in the introduction. We can generalize for 3 orthogonal coordinates:

$$\nabla_D^2 f(r) = \frac{\partial^2}{\partial x^2} + \frac{\alpha_1 - 1}{x} \frac{\partial}{\partial x} + \frac{\partial^2}{\partial y^2} + \frac{\alpha_2 - 1}{y} \frac{\partial}{\partial y} + \frac{\partial^2}{\partial z^2} + \frac{\alpha_3 - 1}{z} \frac{\partial}{\partial z} \quad (2)$$

where $0 < \alpha_1 \leq 1$, $0 < \alpha_2 \leq 1$, $0 < \alpha_3 \leq 1$ and $\alpha_1 + \alpha_2 + \alpha_3 = 3$

For single variable Laplacian operator in fractional space:

$$\nabla_D^2 f(r) = \frac{\partial^2}{\partial x^2} + \frac{\alpha - 1}{x} \frac{\partial}{\partial x} = |\nabla_\alpha| \mathbf{u}_x \quad (3)$$

Using binomial series, ignoring terms involving second or higher degree of x , we obtain:

$$\nabla_\alpha = \left(\frac{d}{dx} + \frac{1}{2} \frac{\alpha - 1}{x} \right) \mathbf{u}_x, \quad 0 < \alpha \leq 1 \quad (4)$$

where \mathbf{u}_x is the unitary vector of x direction.

3. Application

Let consider the Newton's low in one-dimensional fractional space:

$$\frac{d^2 x(t)}{dt^2} = -\frac{1}{m} \nabla_\alpha U(x) \quad (5)$$

where m is a mass and $U(x)$ is a potential function. Let as an example, $m = 1$ and the potential function

$$U(x) = -x + 1 \quad (6)$$

In this condition, the Eq. (5) become:

$$\frac{d^2 x(t)}{dt^2} = - \left(\frac{d}{dx} + \frac{1}{2} \frac{\alpha - 1}{x} \right) (-x + 1) \quad (7)$$

After some algebraic manipulations we obtain:

$$x(t)x''(t) - \frac{\alpha + 1}{2}x(t) + \frac{\alpha - 1}{2} = 0 \quad (8)$$

Solving this equation using MATHEMATICA 8, for initial conditions

$$x(0) = 0.1, \quad x'(0) = 0 \quad (9)$$

we can obtain the solutions for different values of α . In Fig.1 we present these solution in the form of speed, for three different values of $\alpha = 0.3, 0.7, 1$.

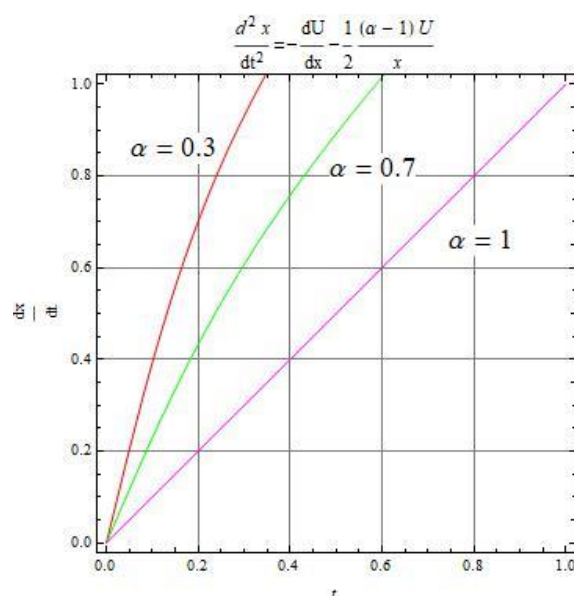


Fig. 1 – The dependence of the speed $x'(t)$ for three different values of fractal dimension α .

3. Conclusions

The main conclusion of the present paper is the following:

i) The expression of the fractional Nabla operator in three dimensional space was given.

ii) In the one dimensional space, the speed dependence of time, for various fractal dimension is obtained. The standard (*i.e.* non-fractal) case, corresponding to the uniform accelerated motion, is obtained for $\alpha = 1$. For $\alpha < 1$, which represent the fractal case, we have the dissipative systems.

REFERENCES

Stillinger F.H., *Axiomatic Basis for Spaces with Noninteger Dimension*, Journal of Mathematical Physics, **18**, 6, 1224-1234 (1977).

GENERALIZAREA OPERATORULUI NABLA ÎNTR-UN SPAȚIU UNIDIMENSIONAL FRAȚIONAL

(Rezumat)

Operatorul Nabla definit pentru un spațiu unidimensional, de dimensiune fracționară, poate fi folosit pentru a modela diverse sisteme cu pierderi, așa cum se demonstrează în aplicația din lucrare.

BULETINUL INSTITUTULUI POLITEHNIC DIN IAȘI
Publicat de
Universitatea Tehnică „Gheorghe Asachi” din Iași
Volumul 63 (67), Numărul 3, 2017
Secția
MATEMATICĂ. MECANICĂ TEORETICĂ. FIZICĂ

FRACTAL ENTANGLEMENT

BY

IRINEL CASIAN BOTEZ^{1,*} and MARICEL AGOP²

“Gheorghe Asachi” Technical University of Iași,

¹Faculty of Electronics, Telecommunication and Information Technology

²Department of Physics

Received: October 18, 2017

Accepted for publication: November 22, 2017

Abstract. In this article we present a generalization of Schrödinger equation, which we named fractal Schrödinger equation, and an generalization of notion of entanglement: fractal entanglement.

Keywords: fractal wave function; entanglement; fractal entanglement.

1. Introduction

Structures of the nature can be assimilated to complex systems, taking into account both their functionality, as well as their structure (Remo Badii 1997; Mitchell, 2011). The models commonly used to study the dynamics of complex systems are based on the assumption, otherwise unjustified, of the differentiability of the physical quantities that describe it, such as density, momentum, energy etc. - for a mathematical model see (Hou Thomas, 2009; Deville and Gatski, 2012) and for some applications, see (Rabinovich and Kalman, 2008; Zhang *et al.*, 2009). The success of differentiable models must be understood sequentially, *i.e.* on domains large enough that differentiability and integrability are valid.

*Corresponding author; *e-mail*: irinel_casian@yahoo.com

But differential method fails when facing the physical reality, with non-differentiable or non-integral physical dynamics, such as instabilities in the case of dynamics of complex structures instabilities that can generate both chaos and patterns.

In order to describe such physical dynamics of structures under severe plastic deformation, but still remaining tributary to a differential hypothesis, it is necessary to introduce, in an explicit manner, the scale resolution in the expressions of the physical variables that describe these dynamics and, implicitly, in the fundamental equations of “evolution” (for example, density, momentum and energy equations). This means that any dynamic variable, dependent, in a classical meaning, on both spatial coordinates and time (Batchelor, 2000), becomes, in this new context, dependent also on the scale resolution. In other words, instead of working with a dynamic variable, described through a strictly non-differentiable mathematical function, we will just work with different approximations of that function, derived through its averaging at different resolution scales. Consequently, any dynamic variable acts as the limit of a functions family, the function being non-differentiable for a null scale resolution and differentiable for a nonzero scale resolution.

This approach, well adapted for applications in the field of physics, where any real determination is conducted at a finite scale resolution, clearly implies the development both of a new geometric structure and of a physical theory (applied to complex structures) for which the motion laws, invariant to spatial and temporal coordinates transformations, are integrated with scale laws, invariant at scale transformations. Such a theory that includes the geometric structure based on the above presented assumptions was developed in the Scale Relativity Theory (Nottale, 2011) and more recently in the Extended Scale Relativity Theory (Agop *et al.*, 2015). Both theories define the “fractal physics models” class (Nottale 1989; Nottale 2010; Nottale 2011; Naschie *et al.*, 1995). In these models the differentiability in the dynamics of complex system is replaced by non-differentiability (fractality). Then the motions constrained on continuous, but differentiable curves in an Euclidian space are replaced with free motions, without any constrains, on fractal curves in a non-differentiable (fractal) space. Thus, the motion curves have double identity: trajectories of the fractal space and streamlines of a fractal fluid (Agop *et al.*, 2015). In such conjecture, for time scale resolution that prove to be large when compared with the inverse of the highest Lyapunov exponent (Mandelbrot, 1983), the trajectories are replaced by “potential” trajectories, so that the concept of “definite positions” is substituted by that of “probability density”. Moreover, the complex system structural units (for example, the particles of a fluid) are substituted with the trajectories (geodesics) themselves so that any external constrains are interpreted as a selection of trajectories (geodesics) by means of measuring device.

2. Mathematical Model

Supposing that the motions of the structural units of the complex systems take place on fractal curves, the following consequences result (Nottale, 2011):

i) Any fractal curve of complex system structural units is explicitly scale resolution dependent δt . Its length becomes infinity when δt goes to zero;

We mention that a curve is a fractal if it satisfies the Lebesgue theorem (Mandelbrot, 1983), *i.e.* its length tends to infinity when the scale resolution becomes zero. Consequently, in this limit, a fractal curve is self-similar: every point reflect, the whole which can be translated into a property of holography (Mandelbrot, 1983).

ii) Through the substitution principle, δt will be identified with dt , *i.e.*, $\delta t = dt$ so that, it will be considered as an independent variable.

iii) The dynamics of the structural units of the complex systems are described through fractal variables. Then, these variables are functions depending on both the space-time coordinates and the scale resolution since the infinitesimal time reflection invariance of any fractal variable is broken. So, in any point of the fractal curve, two derivatives of the variable field $Q(t, dt)$ are defined:

$$\begin{aligned} \frac{d_+ Q(t, dt)}{dt} &= \lim_{\Delta t \rightarrow 0_+} \frac{Q(t + \Delta t, \Delta t) - Q(t, \Delta t)}{\Delta t} \\ \frac{d_- Q(t, dt)}{dt} &= \lim_{\Delta t \rightarrow 0_-} \frac{Q(t, \Delta t) - Q(t - \Delta t, \Delta t)}{\Delta t} \end{aligned} \quad (1)$$

The “+” sign corresponds to forward physical processes of complex system’s structural unit, while the “-” sign correspond to the backwards ones;

iv) The differential of the spatial coordinate $dX^i(t, dt)$ is expressed as the sum of the two differentials, *i.e.*:

$$d_{\pm} X^i(t, dt) = d_{\pm} x^i(t) + d_{\pm} \xi^i(t, dt); \quad (2)$$

The differential part, $d_{\pm} x^i(t)$, is scale resolution independent, while the fractal one, $d_{\pm} \xi^i(t)$, is scale resolution dependent.

v) The non-differentiable part of the spatial coordinate satisfies the equation (Mandelbrot, 1983):

$$d_{\pm}\xi^i(t, dt) = \lambda_{\pm}^i (dt)^{1/D_F} \quad (3)$$

where λ_{\pm}^i are constant coefficients. By means of these coefficients, the fractalization type is specified, while by means of D_F the fractal dimension of the motion curves is defined.

In our opinion, the physical processes characterising both local and global properties of the complex systems imply dynamics on geodesics with various fractal dimensions. The diversity of the fractal dimensions of the geodesics have as a result the assimilation of the complex system with a multifractal (Mandelbrot, 1983). In such conjecture, for $D_F = 2$, the complex system dynamics are described by quantum type processes. For $D_F < 2$ the complex system dynamics are described by correlative type processes, while for $D_F > 2$ the complex system dynamics are described by non-correlative type processes - for details see (Nottale, 1989; Naschie *et al.*, 1995).

vi) The infinitesimal time reflection invariance of any fractal variable is recovered by summing the derivatives d_+/dt and d_-/dt in the non-differentiable operator (fractal operator):

$$\hat{d} = \frac{1}{2} \left(\frac{d_+ + d_-}{dt} \right) - \frac{i}{2} \left(\frac{d_+ - d_-}{dt} \right) \quad (4)$$

This is the result of the Cresson's prolongation procedure applied to the dynamics of the complex system (Cresson, 2006). For example, the non-differentiable operator to the spatial coordinate yields the complex velocity field of the complex system.

$$\hat{V}^i = \frac{\hat{d}X^i}{dt} = V_D^i - V_F^i \quad (5)$$

with

$$V_D^i = \frac{1}{2} \frac{d_+ X^i + d_- X^i}{dt}, \quad V_F^i = \frac{1}{2} \frac{d_+ X^i - d_- X^i}{dt} \quad (6)$$

The real part V_D^i of the complex velocity field is differentiable and scale resolution independent (we shall call it the differentiable velocity field), while

the imaginary part of the complex velocity field, V_F^i , is non-differentiable and scale resolution dependent (we shall call it fractal velocity field);

vii) An infinite number of geodesics can be found relating any pair of points of a fractal manifold in the absence of any external constrain. Then, the infinity of geodesics in the bundle, together with their non-differentiability and the two values of the derivative (see Eqs. (1)-(3)) imply a description of the complex system structural units dynamics by means of a generalized statistical fluid dynamics (fractal fluid description). In such conjecture, the average values of the fractal variables must be considered in the previously mentioned sense. For example, the differential average values of the spatial coordinates is given by the relation:

$$\langle d_{\pm} X^i \rangle \equiv d_{\pm} X^i \quad (7)$$

with

$$\langle d_{\pm} \xi^i \rangle = 0 \quad (8)$$

The relation (8) implies that the differential average values of the spatial coordinates is null.

viii) The complex system dynamics can be described through a scale covariant derivative, the explicit form of which is obtained as follows. Let us consider that the motion fractal curves are immersed in a 3-dimensional space and that X^i are the spatial coordinate of a point on such a curve. We also consider the field $Q(X^i, t)$ and its Taylor's expansion up to the second order:

$$Q(X^i, t) = \partial_t Q dt + \partial_i Q dX^i + \frac{1}{2} \partial_i \partial_k Q dX^i dX^k \quad (9)$$

The functionalities of the relation (9) are valid in any point and more for the points X^i on the fractal curve which we have selected in (9). In these conditions, the forward and backward expressions of the field, Q , from (9) become

$$d_{\pm} Q = \partial_t Q dt + \partial_i Q d_{\pm} X^i + \frac{1}{2} \partial_i \partial_k Q d_{\pm} X^i d_{\pm} X^k \quad (10)$$

We assume that the average values of the all field Q and its derivatives coincide with themselves. Moreover, the differentials $d_{\pm}X^i$ and dt are independent. Then, the average of their products coincides with the product of averages. Consequently, (10) becomes

$$d_{\pm}Q = \partial_i Q dt + \partial_i Q \langle d_{\pm}X^i \rangle + \frac{1}{2} \partial_i \partial_k Q \langle d_{\pm}X^i d_{\pm}X^k \rangle \quad (11)$$

Even the differential average value of $d_{\pm}\xi^i$ is null, for the higher order of $d_{\pm}\xi^i$ the situation can still be different. Let us focus on the average values of the differentials $\langle d_{\pm}\xi^l d_{\pm}\xi^k \rangle$. Using (3) we can write:

$$\langle d_{\pm}\xi^l d_{\pm}\xi^k \rangle = \pm \lambda_{\pm}^l \lambda_{\pm}^k (dt)^{(2/D_F)-1} dt \quad (12)$$

where we consider that the sign $+$ corresponds to $dt > 0$ and the sign $-$ corresponds to $dt < 0$

In these conditions, (11) takes the form:

$$d_{\pm}Q = \partial_i Q dt + \partial_i Q d_{\pm}X^i + \frac{1}{2} \partial_i \partial_k Q d_{\pm}x^i d_{\pm}x^k \pm \frac{1}{2} \partial_i \partial_k Q \left[\lambda_{\pm}^l \lambda_{\pm}^k (dt)^{(2/D_F)-1} dt \right] \quad (13)$$

Multiplying the relation (13) by $(dt)^{-1}$ and neglecting the terms that contain differential factors we obtain (see the method from (Agop *et al.*, 2015)):

$$\frac{d_{\pm}Q}{dt} = \partial_i Q + v_{\pm}^i \partial_i Q \pm \frac{1}{2} \lambda_{\pm}^l \lambda_{\pm}^k (dt)^{(2/D_F)-1} \partial_i \partial_k Q \quad (14)$$

where

$$v_{\pm}^i = d_{\pm}x^i / dt$$

From here, the following operators can be defined:

$$\frac{d_{\pm}}{dt} = \partial_t + v_{\pm}^i \partial_i \pm \frac{1}{2} \lambda_{\pm}^l \lambda_{\pm}^k (dt)^{(2/D_F)-1} \partial_l \partial_k \quad (15)$$

Now, taking into account (4), (5) and (15), let us calculate the fractal operator \hat{d}/dt . It results:

$$\frac{\hat{d}Q}{dt} = \partial_i Q + \hat{V}^i \partial_i Q + \frac{1}{4} (dt)^{(2/D_F)-1} D^{lk} \partial_l \partial_k Q \quad (16)$$

where

$$\begin{aligned} D^{lk} &= d^{lk} - i\bar{d}^{lk} \\ d^{lk} &= \lambda_+^l \lambda_+^k - \lambda_-^l \lambda_-^k, \quad \bar{d}^{lk} = \lambda_+^l \lambda_+^k + \lambda_-^l \lambda_-^k \end{aligned} \quad (17)$$

So, by means of the relation (16) and (17) we can define the scale covariant derivative on the form:

$$\frac{\hat{d}}{dt} = \partial_i + \hat{V}^i \partial_i + \frac{1}{4} (dt)^{(2/D_F)-1} D^{lk} \partial_l \partial_k \quad (18)$$

Let us now consider the functionality of the following scale covariance principle: the physics laws are invariant with respect to scale transformations. In these conditions, the passage from the classical physics to the fractal physics can be implemented by replacing the time derivative d/dt by the fractal operator \hat{d}/dt . For example, applying the operator (18) to the complex velocity field (5), in the absence of any external constraint, the geodesics equation take the form:

$$\frac{\hat{d}\hat{V}^i}{dt} = \partial_i \hat{V}^i + \hat{V}^l \partial_l \hat{V}^i + \frac{1}{4} (dt)^{(2/D_F)-1} D^{lk} \partial_l \partial_k \hat{V}^i = 0 \quad (19)$$

It results that the acceleration, $\partial_i \hat{V}^i$, the convection, $\hat{V}^l \partial_l \hat{V}^i$, and the dissipation, $D^{lk} \partial_l \partial_k \hat{V}^i$, make their balance in any point of the motion fractal curve. The existence of the complex coefficient of viscosity-type $4^{-1} (dt)^{(2/D_F)-1} D^{lk}$ in the dynamics of the complex systems specifies that it is a rheological medium. So, it has memory.

For fractalisation by Markov type stochastic processes (Mandelbrot, 1983; Nottale, 2010), we have:

$$\lambda_+^i \lambda_+^l = \lambda_-^i \lambda_-^l = 2\lambda \delta^{il} \quad (20)$$

where δ^{il} is the Kronecker's pseudo-tensor.

Under these conditions, the geodesics equation takes the simple form:

$$\frac{d\hat{V}^i}{dt} = \partial_i \hat{V}^i + \hat{V}^l \partial_l \hat{V}^i - i\lambda (dt)^{(2/D_F)-1} \partial^l \partial_l \hat{V}^i = 0, \quad i=1,2,3 \quad (21)$$

or in vectorial form:

$$\frac{d\hat{V}}{dt} = \partial_i \hat{V} + (\hat{V} \cdot \nabla) \hat{V} - i\lambda (dt)^{(2/D_F)-1} \Delta \hat{V} = 0 \quad (22)$$

If the motion of the structural units in complex system is supposed irrotational, *i.e.* $\nabla \times \hat{V} = \mathbf{0}$, we can choose \hat{V} of the form:

$$\hat{V} = \nabla \phi \quad (23)$$

where ϕ is a complex velocity potential. Moreover, choosing this potential in the form:

$$\phi = -i\lambda (dt)^{(2/D_F)-1} \ln \psi \quad (24)$$

and substituting it in (22), it results:

$$\lambda (dt)^{(2/D_F)-1} \Delta \psi + i \partial_t \psi = 0 \quad (25)$$

up to an arbitrary phase factor which may be set to zero by a suitable choice of the phase of ψ (see details in (Agop *et al.*, 2015)).

For motions of the structural units of complex system on Peano's curves, $D_F = 2$, and at Compton scale, $\lambda = \hbar/2m_0$, with \hbar the reduced Planck constant, $\hbar = h/2\pi$, and m_0 the rest mass of the entities of complex system, the relation (25) becomes the standard Schrödinger equation:

$$\frac{\hbar}{2m_0} \Delta \psi + i \frac{\partial \psi}{\partial t} = 0 \quad (26)$$

We conclude, in this stage, that the standard Schrödinger Eq. (26) is a particular case of a more general case represented by the Eq. (25), named in this paper *fractal Schrödinger equation*.

3. Entanglement

In 1935 Einstein, in a famous article (Einstein *et al.*, 1935), proceeds from the principle that in a complete theory there must be an element that corresponds to each element of reality and demonstrates that in quantum mechanics the description of reality by its Schrödinger wave function is not complete.

In the same year, in another article, Schrödinger (Schrödinger, 1935) argues that starting from the same wave function interpretation which express the probability relationship between two separate daughter systems, we can introduce the notion of entanglement. By this, Schrödinger understands a new quantum state for each of the two systems, acquired by these once they were in contact. This new state of each system is maintained even after the two systems have been separated in space as much as possible. It has the character like that two states are twin, the modification of the state of one instantly causing the alteration of the state of the other, without being involved any energy transfer.

In 1952, Bohm (Bohm 1952a; Bohm 1952b) interprets this special quantum state as the expression of a hidden quantum variable, but in 1966, Bell (Bell, 1966) demonstrates that the existence of the hidden variable is impossible, and that it is only a new type of quantum state which have to be considered. The existence of this special quantum state can be demonstrated by checking some inequalities.

In 1993, Bennett (Bennett *et al.*, 1993) shows that this kind of quantum state, the entanglement, can be used as an intrinsic encryption method of quantum information (information encoded using the quantum bits - qbits).

4. Conclusions

Taking into account the conclusion of paragraph 3 and the considerations in paragraph 4, we conclude that:

i) The existence of a fractal Schrödinger's equation, whose solution is the fractal wave function, allows us to introduce the generalizing notion of fractal entanglement.

ii) Fractal Entanglement is an intrinsic method of encrypting information transmitted by fractal bits.

REFERENCES

- Agop M., Casian Botez I. *et al.*, *On the Memorizing Ability of Nanostructures*, Journal of Computational and Theoretical Nanoscience, **12**, 4, 682-688 (2015).
Batchelor G.K., *An Introduction to Fluid Dynamics*, Cambridge University Press. (2000).

- Bell J.S., *On the Problem of Hidden Variables in Quantum Mechanics*, Reviews of Modern Physics, **38**, 3, 447-452 (1966).
- Bennett C.H., Brassard G. *et al.*, *Teleporting an Unknown Quantum State via Dual Classical and Einstein-Podolsky-Rosen Channels*, Physical Review Letters, **70**, 13, 1895-1899 (1993).
- Bohm D., *A Suggested Interpretation of the Quantum Theory in Terms of "Hidden" Variables. I*, Physical Review, **85**, 2, 166-179 (1952a).
- Bohm D., *A Suggested Interpretation of the Quantum Theory in Terms of "Hidden" Variables. II*, Physical Review, **85**, 2, 180-193 (1952b).
- Cresson J., *Non-Differentiable Deformations of \mathbb{R}^n* , International Journal of Geometric Methods in Modern Physics, **03**, 07, 1395-1415 (2006).
- Deville M., Gatski T.B., *Mathematical Modeling for Complex Fluids and Flows*, Springer-Verlag Berlin Heidelberg (2012).
- Einstein A., Podolsky B. *et al.*, *Can Quantum-Mechanical Description of Physical Reality Be Considered Complete?*, Physical Review, **47**, 10, 777-780 (1935).
- Hou Thomas L.C., *Multi-Scale Phenomena in Complex Fluids: Modeling, Analysis and Numerical Simulations*, Singapore: World Scientific (2009).
- Mandelbrot B.B., *The Fractal Geometry of Nature*, New York, W.H. Freedman and Company (1983).
- Mitchell M., *Complexity: A Guided Tour*, Oxford University Press (2011).
- Naschie M.S.E., Rossler O.E. *et al.*, *Quantum Mechanics, Diffusion and Chaotic Fractals*, Oxford, Pergamon Press/Elsevier (1995).
- Nottale L., *Fractals and the Quantum Theory of Spacetime*, International Journal of Modern Physics A, **04**, 19, 5047-5117 (1989).
- Nottale L., *Scale Relativity and Fractal Space-Time: Theory and Applications*, Foundations of Science, **15**, 2, 101-152. (2010).
- Nottale L., *Scale Relativity and Fractal Space-Time. A New Approach to Unifying Relativity and Quantum Mechanics*, Imperial College Press, London (2011).
- Rabinovich E., Kalman H., *Generalized Master Curve for Threshold Superficial Velocities in Particle-Fluid Systems*, Powder Technology, **183**, 2, 304-313 (2008).
- Remo Badii A.P., *Complexity: Hierarchical Structures and Scaling in Physics*, Cambridge University Press (1997).
- Schrödinger E., *Discussion of Probability Relations between Separated Systems*, Mathematical Proceedings of the Cambridge Philosophical Society, **31**, 4, 555-563 (1935).
- Zhang S., Kuwabara S. *et al.*, *Simulation of Solid-Fluid Mixture Flow Using Moving Particle Methods*, J. Comput. Physics, **228**, 7, 2552-2565 (2009).

ENTANGLEMENT FRATAL

(Rezumat)

În acest articol prezentăm o generalizare a ecuației lui Schrödinger, pe care am numit-o ecuația fractală a lui Schrödinger, și o generalizare a noțiunii de entanglement: entanglement fractal.

BULETINUL INSTITUTULUI POLITEHNIC DIN IAȘI
Publicat de
Universitatea Tehnică „Gheorghe Asachi” din Iași
Volumul 63 (67), Numărul 3, 2017
Secția
MATEMATICĂ. MECANICĂ TEORETICĂ. FIZICĂ

FUNDAMENTAL ASPECTS OF LASER ABLATION IN LIQUID: GREEN METHOD FOR NANOPARTICLE PRODUCTION

BY

BIANCA CRISTIANA HODOROABĂ^{1,*}

“Alexandru Ioan Cuza” University of Iași,
Faculty of Physics

Received: October 18, 2017

Accepted for publication: November 21, 2017

Abstract. Laser ablation of metallic targets in aqueous media is one of the most powerful tools that we have at this moment for the production of pure and sustainable nanoparticle with direct bio-medical applications. Understanding the fundamental aspects of this process can further pave the way for a better control of the nanoparticle properties and tailoring new pharmaceutical products with direct and localized effects.

Keywords: laser ablation; nanoparticles; liquid; cavitation.

1. General Aspects of Laser Ablation in Liquid

Laser ablation in liquid is coupled with the laser ablation of solids in gaseous media, from the late 80'. The pioneers of this technique are considered Patil *et al.* (Patil *et al.*, 1978) with the group of Needersen *et al.* (Mafune *et al.*, 2000) later reporting themselves the synthetic of colloidal solution through laser ablation of metallic targets in water and organic solvents. In the last two decades laser ablation in liquid has seen a resurgence, now being seen as a low-cost, green, versatile method which allows the synthesis of a wide range of nanoparticles. The versatility of the technique is reflected by the wide range of

*Corresponding author; *e-mail*: bianca.hodoroaba@gmail.com

parameters (properties of the laser beam, properties of the target and those of the liquid solution) that can influence the mechanisms of particle removal, as is the case for vacuum or gas (Compagnini *et al.*, 2003). The particularities of laser ablation in liquid like extreme thermodynamic conditions (high values of the temperature, pressure and particle density), the confinement of the plasma plume by the liquid, the cavitation phenomena, are creating the perfect medium for the production of pure and sustainable chemical products. One main aspect of the whole process is the fact that during expansion the plasma plume resulted as from the interaction of the laser beam and the target contains now not only components from the target but also from the liquid, allowing the formation of nanoparticles with a both crystalline or amorphous structures, that can present themselves as full, hollow or core-shell nanoparticles (NP). The most investigated compounds, are bio compatible metallic NP of Au, Ag or iron oxides.

Their main applications are as passive agents in the administration of the bio-compatible compounds at cellular level and are often used as probes for electronic microscopy.

2. Fundamental Aspect of Laser Ablation in Liquid

For the laser – matter interaction in liquid can be distinguished 4 main parameters whose profile in time and space influences significantly the properties (phase, structure) of the final synthesized products: temperature (T), pressure (p), concentration of the ablated material (CM) and concentration of the solution species (CS). Laser – solid interaction is a complex phenomenon by itself and introducing a new phase (liquid). The main difficulty when investigating this process arises from the semi spherical symmetry of the phenomena, the 4 parameters previously mentioned are not uniformly distributed in space and time.

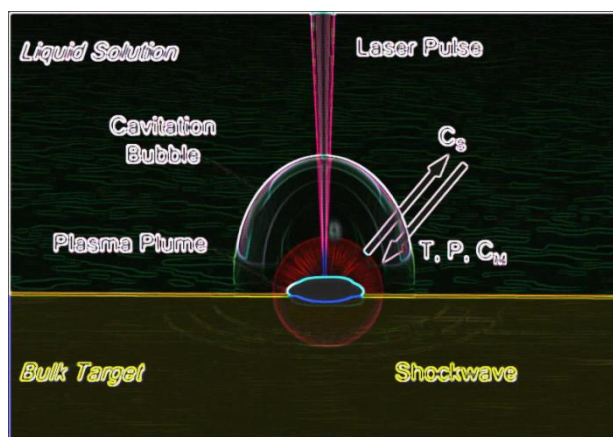


Fig. 1 – Schematic representation of the laser ablation in liquid process (Amendola *et al.*, 2007).

In the process of laser ablation in liquid the primary interaction occurs between the laser pulse and the liquid environment. Therefore, the liquid properties (transparency of the liquid in respect to the laser wavelength, density, thermal conductivity, viscosity, etc.) can induce significant unwanted effects during the irradiation process. The main unwanted effect is the decrease in beam energy that reaches the target's surface.

Nanomaterials synthesis by ultrafast lasers has become a viable method and it constitutes the basis for a new independent science field. Many advantages emerge from using a liquid environment or a liquid film, such as lowering the heat on the target, confining the plasma, and increasing the shock pressure on the surface (Kang *et al.*, 2008; Hwang *et al.*, 2004; Zhang *et al.*, 2017). There is a long range of lasers with different characteristic parameters that can be used in LAL. Regarding the wavelength, in literature we find utilized laser from ultraviolet (UV) (if the liquid allows UV transmission) and visible (VIS) to near – infrared (NIR). The pulse duration can be in the *fs* temporal regime to picosecond, nanosecond, microsecond and millisecond regimes, even extending to continuous – wave lasers (Zhang *et al.*, 2017).

These losses are mainly caused by two phenomena: de-focalization and beam attenuation. The first phenomena, de-focalization, occurs in particular in the case of laser ablation in liquid medium. In contrast with laser ablation in gas, where the focalization conditions are determined just by the position of the target in respect to the focal lens, in LAL the focalization depends on the thickness of the layer of liquid. The de-focalization introduced by the liquid layer is in direct connection with the refractory properties of the solution. In the literature can be found other causes that can affect the focalization, such as vaporization of the liquid at the liquid – air interface and the self – focusing effect. The auto-focusing of the beam is a nonlinear optical phenomenon that occurs in the case of nanosecond and femtosecond laser regimes. The second phenomena (attenuation of the laser beam in the liquid) is due to the photon absorption and scattering on liquid molecules. Worth mentioning consequences of the absorption of the beam's energy are heating of the liquid and/or dissociation of the liquid molecules (in case of the UV lasers). The attenuation is also influenced by the presence of products produced by previous laser beams. The “shielding effect” appears as some collateral phenomena to the ones presented above, basically the already formed NP absorbed a significant part of the incoming beam which lead to the fragmentation and thus to the reduction of the NP dimensions.

The problem of particle removal during the laser matter interaction can be addressed in an analogous manner as in the case of laser ablation in vacuum. An accurate description of the exact ablation mechanisms becomes more difficult here as during the laser-matter interaction more than one mechanism can manifest themselves simultaneously. Thus, we can state here as a general

fact that the main ablation mechanism that are responsible with particle removal and NP formation are evaporation explosive boiling and phase explosion.

3. Expansion and Quenching of the Plasma Plume

In the first picoseconds after the laser pulse interacted with the target the physics is similar to that involved in laser ablation in gas. But, after longer periods of about 10^{-10} - 10^{-9} s an important difference is observed – the liquid strongly confines the plasma near the irradiation point (crater) area (Saka *et al.*, 2000; Perez *et al.*, 2008). The confinement slows down the cooling rate due to the fact that at the interface between the target and the ablated material there is a heat transfer. Maybe one of the most important consequences of the confinement of the plasma is that the ablation yield in liquid is higher compared to the ablation yield in gas. This happens because a larger target area reaches the energetic threshold for ablation (Tsuji *et al.*, 2004; Saka *et al.*, 2000, 2002). Moreover, an essential characteristic of the LAL process emerges from this observation - that the energy transfer is double sided, from the laser pulse to the solid target and from the plasma plume to the already heated target. The plasma– target energy transfer can take place for several nanoseconds after the end of the laser pulse (Mafune *et al.*, 2000; Amendola and Meneghetti, 2009). For moments of time that surpass 10^{-10} s the plasma plume expands in the liquid and cools down by heating the liquid as well as the target. The liquid can reach temperatures of about a few 10^3 K similar to the ones found for plasma generated in vacuum, these temperatures are appropriate for ionization processes and pyrolysis of the solution molecules. The gradients of the T, P, C_M and C_S are becoming more uniform and are defining fast transformation in both space and time for all the main parameters. Qualitative estimation of these gradients can be made using theoretical and experimental techniques while a quantitative evaluation is missing. In this stage the ejected species and liquid ones are mixing (Fig. 2). Now it will take place 4 types of chemical reactions both from a plasma plume perspective as well as the interface between the plasma and the liquid media.

The first type of reactions refers to the formation of metastable phases of the material induced by the extreme conditions within the plasma. The second type of reaction takes places in the plasma volume, here the involved reactants are the ionized species of the target and those of the solution. The species of the solution are particle resulted from the ionization and excitation generated at the interface liquid- plasma (Fig. 2). Thus, on the expansion direction of the plume it appears an area named “plasma-induced plasma” where we initially find the ionized species of the liquid media. This area will evolve while it’s unified with the primary plasma, once it is completely generated. Therefore, the first ablation mechanism like Coulomb explosion will lead to the formation of a plasma region which contains only liquid particle

while with the manifestation of thermal mechanisms and the full generation of the primary plasma plume the two-plasma region and blending leading to a confined plasma plume containing both ionized species of the target and those of the solutions.

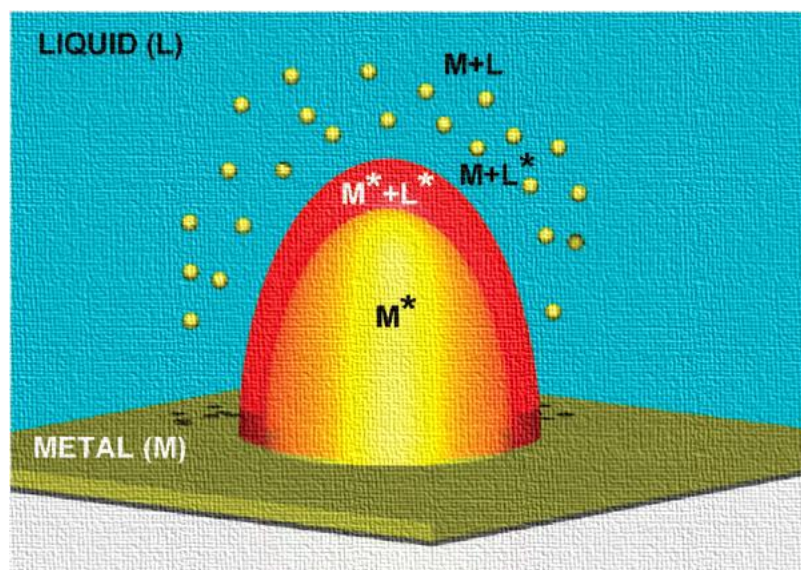


Fig. 2 – Schematic representation of particle distribution during the laser ablation process in liquid (Amendola and Meneghetti, 2013).

The third set of chemical reactions are conducted in the liquid – plasma interface. This is due to the fact that the thermodynamic state characterized by extreme values of the temperature, pressure and particle density, which create the perfect conditions for the chemical interactions between the ejected metallic particles and those of the liquid. The last type of interactions are happening in the liquid media. Due to the elevated values of the pressure at the plasma plume expansion front, the metallic particles will be ejected in the volume of the liquid media where it will interact with the solutions molecules (Yang, 2007). It is worth noting that 3 out of the 4 types of reactions presented here are involving both particles of the target and of the liquid. As such these chemical reactions coupled with the thermodynamic conditions can offer infinite possibilities for the tailoring of new sustainable materials by combining elements from both media (Sakka *et al.*, 2000; Patil *et al.*, 1978; Yang and Wang, 2000).

The main mechanism of nanoparticle formation generated by laser ablation in liquid is represented by nuclei growth. This process is assumed to be manifesting itself during the cooling of the plasma plume, followed by the growth of the supposed nuclei and their fusion (Fig.3).

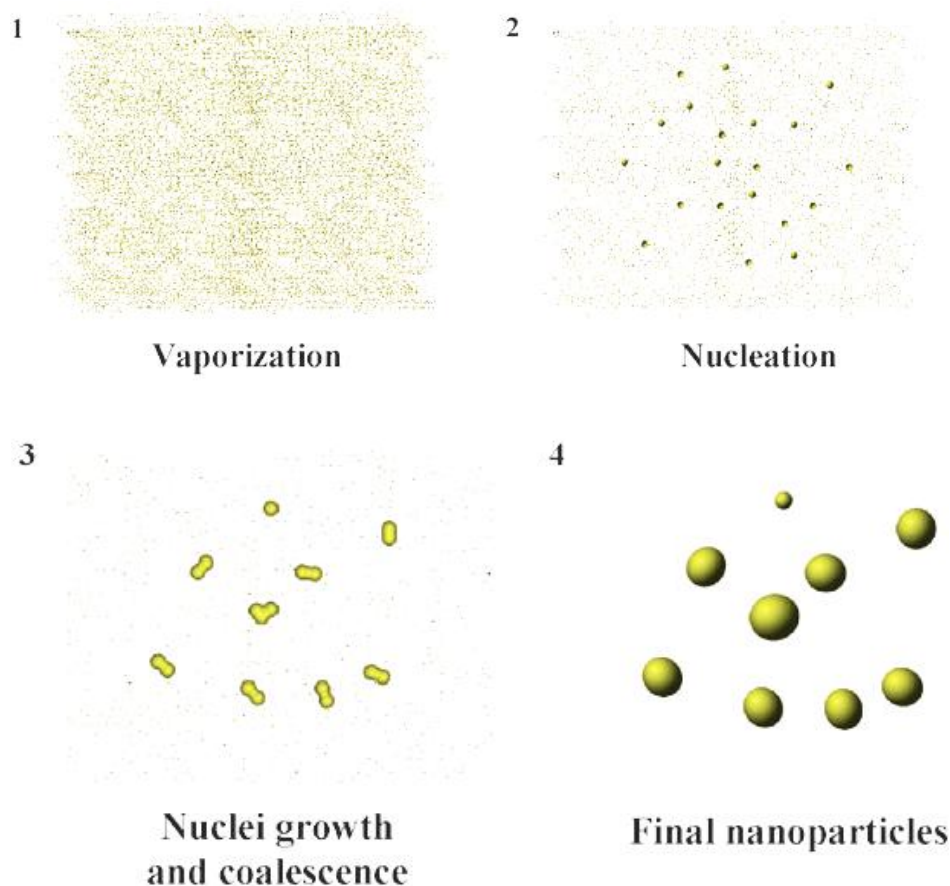


Fig. 3 – Representation of the nanoparticle formation process using the laser ablation in liquid (Amendola and Meneghetti, 2009).

In literature there are three experimental confirmations of this hypothesis. First it is represented by the experimental observation of crystalline structure in nanoparticles generated by laser ablation in liquid (Amendola *et al.*, 2007; Amendola and Meneghetti, 2007). The second one is given by the fact that nanoparticles generated in the presence of ligands or polymeric solutions have a narrower dimensional distribution in comparison with the nanoparticles generated in pure solvents (Mafune *et al.*, 2001, 2000). The third and last main confirmation from literature comes from the results that laser ablation in reactive solvents does not lead to the formation of pure metallic nanoparticles (Sakka *et al.*, 2002).

The nucleation force present inside the plasma volume is given by the supersaturation. This is given by the ratio between the real vaporization pressure p and the equilibrium vaporization pressure $p_0(T)$. The free energy barrier ΔG_N

and the minimum radius R_N are thus depending on the supersaturation as follows:

$$\Delta G_N \propto \left[k_B T \left(\frac{p}{p_0(T)} \right) \right]^{-2}, \quad (1)$$

$$R_N \propto \left[k_B T \left(\frac{p}{p_0(T)} \right) \right]^{-1}, \quad (2)$$

where k_B is the Boltzmann constant, and T is the temperature describing the equilibrium state, while the well-known Gibbs free energy is a measure of the energy of a transformation state in between competing states. For a better understanding of this concept we consider two phase that coexist in the same thermodynamic conditions. Between the two states the one with the lower free energy is steady while the other becomes metastable with the possibility of become a steady state as well. From a thermodynamic perspective the phase transformations are given by the differences in between the values of the free energy.

A major drawback of laser ablation in liquid as a technique for NP generation is the temporal imprecisions in pointing down the starting point of nucleation processes and those of NP formation. The exact moment at which the nucleation process is starting is strongly dependent on the concentration, temperature and pressure. For this reason, why, it cannot be related to the results obtained from laser ablation in gas. Some authors suggest that the nucleation jumpstarts after 10^{-9} s (Wang *et al.*, 2005) while other propose an approximate time of 10^{-5} s (Tsuji *et al.*, 2008; Itina, 2011). However, there is a lack of experimental proofs regarding the NP formation mechanism. It is still not clear if the nucleation and NP growth take place before or after the intensive mixing of the ejected species with those of the liquid. Moreover, due to the limitations of the experimental investigations techniques the correct ionization degree for some species it is difficult to find out. Optical emission spectroscopy confirms the fact that there is a chemical interaction between the species of the target and those of the liquid even in the plasma. On the other hand, this information is not quantitative and thus not truly relevant to the NP formation phenomena.

Laser produced plasmas are complex media which contains besides electrons atoms, multiply ionized ions, atom, clusters also molten material fragments (Amendola and Meneghetti, 2013). Their presence is not negligible as in the past few years the group of Zighilei (Zighilei *et al.*, 2009) has proposed a NP formation mechanism based of the phase explosion and the braking of the material in various structures. That being said there is not a consensus in the literature which could tell us if from these fragments it can result some precursors of NP. Therefore, a hypothesis can be made about these types of structures. The molten material, solid fragments and molecular clusters are directly ejected from the target and they could

constitute preferential sites for the generation and characterization of nuclei. The direct conclusion of this would be in direct connection with the results reported by Zighilei *et al.*, that the nucleation phase is not that relevant for the laser ablation in liquid as a whole, because the nuclei could be directly extracted from the target during the ablation process. In order to clarify this aspect further studies are needed for the understanding of the fundamental mechanism of ablation and material removal in the laser ablation in aqueous media. However, some nanoparticles obtained through this method are mainly polycrystalline thus at some point during the formation and expansion of the plume, the fusion of the nuclei still occurs.

In the framework of laser ablation in liquid, it is also possible the generation in specific conditions of liquid supersaturation of a mixture of clusters and atomic precursors. More precise, the vaporization pressure of the ejected species is higher than the equilibrium one thus the nucleation and growth process are accelerated. The dimensional distribution of the NP generated by laser ablation follows a lognormal function. An exception to this rule is the irradiation of already produced NP. Granqvist *et al.* showed that the NP are described by a log normal dimensional distribution when their growth is given by the diffusion processes of the atoms and nanoparticles which occurs produced simultaneously. The following agglomeration of NP do not affect the distribution as long as the drift moment of the NP is not affected.

The dimension of the produced NP can be controlled with the use of the external experimental parameters like wavelength, pulse duration, repetition frequency irradiated surface and the energy per pulse. As an example here in conditions of identical fluence the NP generated with UV laser beam would favor the formation of reactive species, the use of an IR beam would lead to an uneven energy distribution at the surface as the impurities have a preferential absorption. Finally, the use of a bigger surface would aid the formation of NP with a wider dimensional distribution.

4. Conclusions

Recent developments in laser ablation in liquid have led to the creation of a new exciting research area related to the formation of NP and generation of complex pharmaceutical compounds using one-step technologies. There is however a great need of fundamental research that would eventually allow researcher a better control on the NP distribution and properties. The use of complimentary investigation techniques and the ability to perform in situ investigations of the dynamics of atoms and ions leading into the nuclei formation could be of great help when attempting to clarify this problem.

REFERENCES

- Amendola V., Meneghetti M., *Laser Ablation Synthesis in Solution and Size Manipulation of Noble Metal Nanoparticles*, Phys. Chem. Chem. Phys., **11**, 20, 3805-3821 (2009).
- Amendola V., Polizzi S., Meneghetti M., *Free Silver Nanoparticles Synthesized by Laser Ablation in Organic Solvents and their Easy Functionalization*, Langmuir, **23**, 6766-6770 (2007).
- Amendola V., Meneghetti M., *Controlled Size Manipulation of Free Gold Nanoparticles by Laser Irradiation and their Facile Bioconjugation*, J. Mater. Chem., **17**, 4705-4710 (2007).
- Amendola V., Meneghetti M., *What Controls the Composition and the Structure of Nanomaterials Generated by Laser Ablation in Liquid Solution*, Phys. Chem. Chem. Phys., **15**, 3027 (2013).
- Compagnini G., Scalisi A.A., Puglisi O., *Production of Gold Nanoparticles by Laser Ablation in Liquid Alkanes*, J. Appl. Phys., **94**, 7874 (2003).
- Hwang D.J., Choi T.Y., Grigoropoulos C.P., *Liquid-Assisted Femtosecond Laser Drilling of Straight and Three-Dimensional Microchannels in Glass*, Appl. Phys. A, Mater. Sci. Process., **79**, 605-612 (2004).
- Itina T.E., *On Nanoparticle Formation by Laser Ablation in Liquids*, J. Phys. Chem. C, **115**, 5044-5048 (2011).
- Kang H.W., Lee H., Welch A.J., *Laser Ablation in a Liquid- Confined Environment Using a Nanosecond Laser Pulse*, J. Appl. Phys., **103**, 083101 (2008).
- Mafune F., Kohno J.-Y., Takeda Y., Kondow T., Sawabe H., *Formation and Size Control of Silver Nanoparticles by Laser Ablation in Aqueous Solution*, J. Phys. Chem. B, **104**, 9111-9117 (2000).
- Mafune F., Kohno J., Takeda Y., Kondow T., Sawabe H., *Formation of Gold Nanoparticles by Laser Ablation in Aqueous Solution of Surfactant*, J. Phys. Chem. B, **105**, 5114-5120 (2001).
- Patil P.P., Phase D.M., Kulkarni S.A., Ghaisas S.V., Kulkarni S.K., Kanetkar S.M., Ogale S.B., Bhide V.G., *Pulsed-Laser-Induced Reactive Quenching at Liquid-Solid Interface: Aqueous Oxidation of Iron*, Phys. Rev. Lett., **58**, 238-241 (1978).
- Perez D., Beland L.K., Deryng D., Lewis L.J., Meunier M., *Numerical Study of the Thermal Ablation of Wet Solids by Ultrashort Laser Pulses*, Phys. Rev. B: Condens. Matter Mater. Phys., **77**, 014108 (2008).
- Sakka T., Iwanaga S., Ogata Y.H., Matsunawa A., Takemoto T., *Laser Ablation at Solid-Liquid Interfaces: An Approach from Optical Emission Spectra*, J. Chem. Phys., **112**, 8645-8653 (2000).
- Sakka T., Takatani K., Ogata Y.H., Mabuchi M., *Effects of Pulse Duration Upon the Plume Formation by the Laser Ablation of Cu in Water*, J. Phys. D, **35**, 65 (2002).
- Tsuji T., Tsuboi Y., Kitamura N., Tsuji M., *Microsecond-Resolved Imaging of Laser Ablation at Solid-Liquid Interface: Investigation of Formation Process of Nano-Size Metal Colloids*, Appl. Surf. Sci., **229**, 365-371 (2004).

- Yang G.W., Wang J.B., *Carbon Nitride Nanocrystals Having Cubic Structure Using Pulsed Laser Induced Liquid–Solid Interfacial Reaction*, Appl. Phys. A, **71**, 343 (2000).
- Yang G.W., *Laser Ablation in Liquids: Applications in the Synthesis of Nanocrystals*, Progress in Materials Science, **52**, 648-698 (2007).
- Wang C.X., Liu P., Cui H., Yang G.W., *Nucleation and Growth Kinetics of Nanocrystals Formed Upon Pulsed-Laser Ablation in Liquid*, Appl. Phys. Lett., **87**, 201913 (2005).
- Tsuji T., Thang D., Okazaki Y., Nakanishi M., Tsuboi Y., Tsuji M., *Preparation of Silver Nanoparticles by Laser Ablation in Polyvinylpyrrolidone Solutions*, Appl. Surf. Sci., **254**, 5224 (2008).
- Zhigilei L.V., Lin Z., Ivanov D.S., *Atomistic Modeling of Short Pulse Laser Ablation of Metals: Connections between Melting, Spallation, and Phase Explosion*, J. Phys. Chem. C, **113**, 11892-11906 (2009).
- Zhang, D., Gokce B., Barcikowski S., *Laser Synthesis and Processing of Colloids: Fundamentals and Applications*, Chem. Rev., **117**, 3990-4103 (2017).

ASPECTE FUNDAMENTALE ALE
ABLAȚIEI LASER ÎN LICHID: METODA ECOLOGICĂ DE
PRODUCERE A NANOPARTICULELOR

(Rezumat)

În prezent ablația laser în mediul lichid este o tehnică ieftină, versatilă și ecologică ce oferă acces la sintetizarea unei plaje extinse de nanomateriale. Versatilitatea metodei se reflectă profund în plaja largă de parametri (parametri ai laserului, ai lichidului, ai țintei) ce influențează întregul proces de preparare a materialelor. Particularitățile procesului precum: condiții termodinamice “extreme” (valori mari ale temperaturii, presiunii, densității de particule), efectul lichidului de confinare a plasmei, fenomenul de cavitație, furnizează mediul perfect de sintetizare a unor produși puri, sustenabili și ușor funcționalizabili. Mai mult decât atât, în timpul expansiunii în lichid, plasma de ablație înglobează atât particule îndepărtate din material, cât și particule ale soluției. Astfel, pot rezulta nanoparticule atât cu structură cristalină cât și amorfă sub formă de sfere pline, sfere goale sau structuri de tip miez – capsulă ce reprezintă de fapt “semnături” ale ambelor faze (lichid, solid). Această caracteristică a procesului conferă posibilitatea generării in-situ de compuși stabili de tip nanoparticulă – polimer, care nu numai că împiedică agregarea nanoparticulelor pe termen lung, dar mai important astfel se pot produce compuși farmaceutici ce pot fi utilizați în diverse forme.

BULETINUL INSTITUTULUI POLITEHNIC DIN IAȘI
Publicat de
Universitatea Tehnică „Gheorghe Asachi” din Iași
Volumul 63 (67), Numărul 3, 2017
Secția
MATEMATICĂ. MECANICĂ TEORETICĂ. FIZICĂ

RADIOBIOLOGICAL CONSIDERATIONS ON MODERN TECHNIQUES OF EXTERNAL RADIOTHERAPY IMRT AND VMAT

BY

CAMIL CIPRIAN MIREȘTEAN¹, CĂLIN GHEORGHE BUZEA^{1,*} and
DRAGOȘ TEODOR IANCU^{1,2}

¹Regional Institute of Oncology, Iași

²“Grigore T. Popa” University of Medicine and Pharmacy, Iași

Received: October 20, 2017

Accepted for publication: November 24, 2017

Abstract. In the last decades, we witness the advancement of new external radiotherapy techniques together with significant advances in cancer biology, imaging and computerized data processing that impact on the involvement of radiobiological considerations in the therapeutic decision. Preclinical studies demonstrated significant changes in cell survival fractions under irradiation parameters, that simulate irradiation with increased and variable dose rate and total irradiation time/fraction > 30 min, similar to the situation encountered in IMRT irradiation in vitro. Inverse planning techniques allow irradiation with the integrated boost technique, irradiating target sub-volumes with fractions greater than 2Gy. In this context, the use of the linear quadratic model may be useful but requires caution both in assessing equivalent-tumoral doses and acute and late toxicities. The introduction of mathematical models that calculate TCP (tumor control probability) and NTCP (the probability of healthy tissues to develop toxicity) has simplified comparative assessment for complex irradiation plans.

Keywords: radiotherapy; therapeutic decision; inverse planning; linear quadratic model.

*Corresponding author; *e-mail*: calinb2003@yahoo.com

1. Introduction

In the last decades, we have witnessed a steady increase in the use of modern radiotherapy techniques, having as a prerequisite the achievement of a higher degree of target volume covering compared to conformational radiotherapy, but especially the reduction of doses received by radiosensitive organs. With all these advantages, the implementation of modern techniques and the physical characteristics of the radiation beam and the delivery mode of the dose brings a number of uncertainties and challenges regarding the radiobiological effects both on the tumor target and the healthy tissues (Nishimura *et al.*, 2015).

The application of radiobiological modeling originated three decades ago and many research centers have tried to prove the utility of this instrument in clinical practice. However, mathematical models are not perfect because they do not take into account the individual variables of the radiosensitivity of each case, the inclusion of individual clinical biological and imaging parameters being needed to improve their predictive value. Biological modeling uses a DVH of a certain plan and certain biological features (histological type of the tumor and characteristics of the normal tissues from the organs exposed to the risk of toxicity) for the calculation of TCP and NTCP.

Consider a statistical ensemble of tumors treated with radiotherapy with dose D . Let us denote by λ the mean number of surviving clonogenic tumor cells in this tumor ensemble. The TCP is given by the probability of no surviving clonogenic cell. If the actual number of surviving clonogenic cells among the tumors is distributed according to Poisson statistics, then TCP for a tumor is calculated using the Poisson model by the following formula (Nishimura *et al.*, 2015):

$$TCP(D) = \exp(-\lambda(D)) \quad (1)$$

Using the LQ model

$$\lambda(D) = N_0 \exp(-\alpha D - \beta D^2) = N_0 \exp(-\alpha D - \beta dD) \quad (2)$$

where N_0 denotes the initial number of clonogenic cells in the tumor, and the second form corresponds to fractionated irradiation with dose per fraction d and total dose D . The TCP formula of the Poisson model combined with the LQ expression thus reads

$$TCP(D) = \exp(-N_0 \exp(-\alpha D - \beta dD)) \quad (3)$$

The number of clonogenic cells N_0 can be expressed in terms of clonogenic density ρ_0 and tumor volume V

$$N_0 = \rho_0 V \quad (4)$$

The clonogenic density ρ_0 has been estimated from experimental data and/or models at 10^4 - 10^6 cells per cm^3 , significantly below the density of all cells (10^9 cells per cm^3). There is evidence even for the clonogenic density being dependent on tumor volume.

One of the most used models is Lyman-Kutcher-Burman (LKB). In the LKB model, NTCP is defined as:

$$NTCP = \frac{1}{\sqrt{2\pi}} \int_{-\infty}^u e^{-t^2/2} dt \quad (5)$$

where

$$u = \frac{D - TD50(V)}{m \times TD50(V)} \quad (6)$$

$$TD50(V) = TD50(1)/V^n \quad (7)$$

where $TD50(V)$ is the tolerance with 50% probability of complications caused by uniform irradiation in volume V where $TD50$ is the probability of complications in healthy tissue caused by uniform irradiation of volume V and where n is the exponent of the volume and m is a parameter that is inversely proportional to the slope of the dose-response curve (Warkentin *et al.*, 2004).

2. Discussion

For example, Basu *et al.* compares in 10 cases of prostate adenocarcinoma, TCP and NTCP calculated for plans with conventional four-field box techniques, plus conformational boosts with three fields (3D + 3DCRT), 3D-CRT plans followed by IMRT boost (3D + IMRT), IMRT plans followed by IMRT boost (IMRT + IMRT) and simultaneously integrated boost plan (SIBIMRT). In the case of integrated boost, equivalent doses were calculated using the biological equivalent dose, assuming the alpha/beta ratio is 1.5 Gy, and NTCP was calculated using the Lyman-Kutcher-Burman (LKB) model. SIBIMRT provided the lowest NTCP with 3 weeks of reduced treatment time, being considered as a feasible technique for dose escalation (Basu and Bahl, 2009).

Hardcastle *et al.* comparatively evaluate IMRT and VMAT irradiation plans for prostate neoplasm with the objective of assessing the risk of rectal toxicity. With similar coverage of the target volume, the VMAT technique offers a lower risk of late rectal complications (Hardcastle *et al.*, 2011).

Comparative study on plans obtained for the same patients through different techniques has revealed difficulties in assessing the advantages and disadvantages of each and every case. Significant dosimetric differences do not

always translate into advantages in tumor control, the biological properties of tumor and healthy tissue may play an important role in the irradiation response. The TCP and NTCP mathematical models simplify these differences by providing precise values for the possibility of obtaining tumor control and the risk that the treatment will be accompanied by acute and delayed toxicity. In many cases, minimal differences between these values save time-consuming optimization of plans with no benefit in clinical practice. The purpose of increasingly use of radiobiological models was to have a predictive tool for the biological effects of variations of different parameters in the treatment plan, to evaluate the consequence of geometric errors and to compare the plans obtained with modern radiotherapy and those with conventional techniques, to achieve a clinical-benefit dosimetric benefit correlation (Jiang *et al.*, 2013; Mesbahi and Oladghaffari, 2017).

The IMRT technique is characterized by a prolonged delivery time of the irradiation dose per fraction. In a study focused on the delivery effect at different times on the A549 cell line, of the same dose on A549 tumor growth in mice, Jiang and co-workers demonstrate using the formalism of the linear quadratic model and the incomplete lesion repair model to generate cell survival curves. Radiation was delivered with one fraction per day simulating a clinical model. Delivery times over 40 minutes diminished the tumoricidal effects of irradiation but in clinical practice the disadvantage of the risk of cellular repopulation associated with long delivery times of each fraction characteristic to the IMRT technique could be compensated by the radiosensitizing effects of reoxygenation (Jiang *et al.*, 2013; Mesbahi and Oladghaffari, 2017). Another study is aimed at exploring the impact of prolonged dose delivery times similar to IMRT irradiation on (HCC) HepG2 and Hep3B human hepatocellular carcinoma cell line destruction. Simulating dose delivery conditions similar to IMRT technique significantly decreased the effect of HepG2 cell destruction, but not Hep3B. The ability to repair sublethal lesions was the predominant factor determining the decrease of the HepG2 cells tumorigenic randament, effect proven by clinical trials also. Based on the analysis of clinical data, it was concluded that dose-modifying factors of 1.08-1.16 should be considered when total irradiation time is 20-30 min (Zheng *et al.*, 2005, Shibamoto *et al.*, 2012).

The IMRT technique is beneficial to irradiate the sub-volumes from a target volume with different doses/fraction by using the integrated boost. The necessity of evaluating the equivalent dose from the standard fractionation as both tumoricidal and toxicity has led to the need for frequent use of the linear-quadratic model ($n_2d_2/n_1d_1 = (1 + d_1/[a/b]) / (1 + d_2/[a/b])$) (where d_1 and d_2 are doses per fraction and n_1 and n_2 the number of fractions). The Linear Quadratic Model is useful for converting between relatively low dose fractions used in conventional radiotherapy, but studies have shown errors in assessing the equivalent dose for large fraction of doses per day or for a small number of fractions. The validity of its use for hypofractionation schemes, stereotactic radiosurgery or single session irradiation should be validated by clinical trials (Brenner, 2008).

Guerrero and Li propose a modified version of the modified linear quadratic model for evaluating equivalent doses in extracranial stereotactic radiosurgery by evaluating the proposed equation for doses $>15\text{Gy}$. The new parameter introduced is valid in vitro, on the cell survival curves of several human tumor cell lines and in vivo for animal-validated iso-effect curves. For high dose per fraction, the modified linear quadratic model appears to provide predictive accuracy and correspondence with the clinical reality superior to the linear quadratic model for calculating the isoeffect dose (Guerrero and Li, 2004).

At low doses per fraction ($<1\text{Gy}$), the hyper-radiosensitization effect described in both tumor and healthy tissue may result in underestimating the response to treatment and toxicity using the linear quadratic model. It is the case of IMRT and VMAT techniques in which large volumes of tissue are irradiated with doses per fraction situated in this interval characteristic to the effect of hyper-radiosensitization. Validation of some equations that more accurately characterize the small dose per fraction effects on cells, opens new horizons of approaching radioresistant tumors at doses of 2Gy . Joiner, Marples *et al.* describe that most cell lines have hyper-radiosensitivity (HRS) at very low doses of radiation ($<10\text{ cGy}$) and around 30 cGy , increases the radioresistance (IRR), around 1 Gy/fraction , the radioresistance becomes maximum (Joiner *et al.*, 2001).

3. Conclusions

Technological development, the implementation of intensity modulated techniques and the image guided radiotherapy led to the increase of reproducibility of the treatment plans and irradiation accuracy. From a radiobiological point of view, the use of high dose rates, long dose delivery times, and dose distribution in healthy tissue volumes (reducing high dose irradiated volumes and increasing volumes that will receive low doses) are factors that alter cell survival curves and it is necessary to validate the mathematical models through clinical studies. The use of TCP and NTCP can provide an intuitive solution in the selection and comparison of different treatment plans in terms of tumor control and toxicity.

REFERENCES

- Basu K.S., Bahl A., *Normal Tissue Complication Probability: Does Simultaneous Integrated Boost Intensity-Modulated Radiotherapy Score over Other Techniques in Treatment of Prostate Adenocarcinoma*, J. Cancer Res. Ther., Apr-Jun, **5**, 2, 78-84 (2009).
- Brenner D.J., *The Linear-Quadratic Model is an Appropriate Methodology for Determining Iso-Effective Doses at Large Doses per Fraction*, Semin. Radiat. Oncol., **18**, 234-239 (2008).

- Guerrero M., Li X.A., *Extending the Linear-Quadratic Model for Large Fraction Doses Pertinent to Stereotactic Radiotherapy*, Phys. Med. Biol., Oct 21, **49**, 20, 4825-4835 (2004).
- Hardcastle N., Tomé W.A., Foo K. *et al.*, *Comparison of Prostate IMRT and VMAT Biologically Optimized Treatment Plans*, Med. Dosim., Autumn, **36**, 3, 292-298 (2011).
- Jiang L., Xiong X.P., Hu C.S. *et al.*, *In Vitro and in Vivo Studies on Radiobiological Effects of Prolonged Fraction Delivery Time in A549 Cells*, J. Radiat. Res., Mar, **54**, 2, 230-234 (2013).
- Joiner M.C., Marples B., Lambin P. *et al.*, *Low-Dose Hypersensitivity: Current Status and Possible Mechanisms*, Int. J. Radiat. Oncol. Biol. Phys., Feb. 1, **49**, 2, 379-389 (2001).
- Mesbahi A., Oladghaffari M., *An Overview on the Clinical Application of Radiobiological Modeling in Radiation Therapy of Cancer*, Int. J. Radiol. Radiat. Ther., **2**, 1, 00013 (2017).
- Nishimura Y., Komaki R., *Intensity-Modulated Radiation Therapy, Clinical Evidence and Techniques*, Tokio: Springer, 2015.
- Shibamoto Y., Otsuka S., Iwata H. *et al.*, *Radiobiological Evaluation of the Radiation Dose as Used in High-Precision Radiotherapy: Effect of Prolonged Delivery Time and Applicability of the Linear-Quadratic Model*, J. Radiat. Res., **53**, 1-9 (2012).
- Warkentin B., Stavrev P., Stavreva N., Field C., Fallone B.G., *A TCP-NTCP Estimation Module Using DVHs and Known Radiobiological Models and Parameter Sets*, J. Appl. Clin. Med. Phys., **5**, 1, 50-63(2004).
- Zheng X.K., Chen L.H., Yan X. *et al.*, *Impact of Prolonged Fraction Dose-Delivery Time Modeling Intensity-Modulated Radiationtherapy on Hepatocellular Carcinoma Cell Killing*, World J. Gastroenterol., Mar 14, **11**, 10, 1452-1456 (2005).

CONSIDERAȚII RADIOBIOLOGICE ASUPRA TEHNICILOR MODERNE DE RADIOTERAPIE EXTERNĂ IMRT ȘI VMAT

(Rezumat)

În ultimele decade asistăm la un avânt al noilor tehnici de radioterapie externă simultan cu progrese semnificative înregistrate în biologia cancerului, în imagistica și în prelucrarea computerizată a datelor cu impact asupra implicării raționamentelor radiobiologice în decizia terapeutică. Studiile preclinice au demonstrat modificări semnificative în fracțiile de supraviețuire celulară în condițiile parametrilor de iradiere care simulează o iradiere în pulsuri cu debit crescut și cu timp total de iradiere/fracțiune > 30 minute asemănător situației întâlnite în iradierea IMRT in vitro. Tehnicile de planificare inversă permit iradierea prin tehnica boostului integrat, iradiind subvolume din ținta cu fracțiuni mai mari de 2Gy. Utilizarea modelului liniar pătratic în acest context poate fi utilă, dar necesită precauții atât în evaluarea dozelor echivalente tumorice cât și al toxicităților acute și tardive. Introducerea modelelor matematice care calculează TCP (probabilitatea de control tumoral) și NTCP (probabilitatea țesuturilor sănătoase de a dezvolta toxicități) a simplificat evaluarea comparativă a planurilor complexe.

BULETINUL INSTITUTULUI POLITEHNIC DIN IAȘI
Publicat de
Universitatea Tehnică „Gheorghe Asachi” din Iași
Volumul 63 (67), Numărul 3, 2017
Secția
MATEMATICĂ. MECANICĂ TEORETICĂ. FIZICĂ

**A COMPUTER APPLICATION FOR THE PREDICTION OF
RISK OF DYSPHAGIA IN THE IRRADIATION
OF HEAD AND NECK CANCER**

BY

**CĂLIN GHEORGHE BUZEA^{1,*}, CAMIL CIPRIAN MIREȘTEAN¹ and
DRAGOȘ TEODOR IANCU^{1,2}**

¹Regional Institute of Oncology Iași

²“Grigore T. Popa” University of Medicine and Pharmacy, Iași

Received: October 20, 2017

Accepted for publication: November 24, 2017

Abstract. Dysphagia is a severe late complication in radiotherapy of head and neck cancer. Aspiration associated risk, weight loss and affecting the quality of life are just a few of the consequences. Dose limitation at the pharyngeal constrictors and larynx for the radio-treated patients with locally advanced head and neck cancers decreases the risk of late dysphagia.

Radiobiological model proposed by Christianen *et al.* for evaluation of late dysphagia can provide a good prognostic by calculation of NTCP (normal tissue complication probability) values, using the median dose received by the supraglottic larynx and superior pharyngeal constrictor muscles contoured as OARs (organs at risk). We designed a simple Microsoft Windows computer application for calculation in a simple way the risk of post radiotherapy dysphagia in neoplasms of the head and neck.

Keywords: dysphagia; radiobiological model; NTCP; computer application; head and neck cancer.

*Corresponding author; *e-mail*: calinb2003@yahoo.com

1. Introduction

Radiotherapy-induced dysphagia became a common complication in patients receiving high-dose radiotherapy as a part of the multimodal treatment of head and neck cancers. Nearly 50% report this distressing symptom a year after treatment completion (Roe *et al.*, 2014). Dose limitation at the pharyngeal constrictors and larynx for the radio-treated patients with locally advanced head and neck cancers decreases the risk of late dysphagia.

Treatments intensifications in head and neck cancers had led to improvement the prognostic but also to a high rate of mucosal and pharyngeal toxicity. The resulting impaired swallowing can lead to severe complications like aspiration pneumonia. For clinicians it is important to identify patients with the potential risk of dysphagia to prevent related complications (malnutrition, aspiration) and to provide supportive treatment for this purpose (Denaro *et al.*, 2013).

Radiobiological model proposed by Christianen *et al.* for evaluation of late dysphagia can provide a good prognostic by calculation NTCP (normal tissue complication probability) values using the median dose received by the supraglottic larynx and superior pharyngeal constrictor muscles contoured as OARs (organs at risk)

$$NTCP = (1 + e^{-S})^{-1}$$

where $S = -6.09 + (D_{\text{mean constrictor faringian superior}} * 0.057 + D_{\text{mean laringe supraglottic}} * 0.037)$.

2. Materials and Methods

For 3 patients with locally advanced oropharyngeal cancer treated with the VMAT technique the upper pharyngeal constrictor and the supraglottic larynx were subsequently contoured (Fig. 1) and D_{mean} (mean dose) was evaluated. All patients were treated with 3 cycles of Carboplatin-Paclitaxel induction chemotherapy. The treatment plan was performed on a CT-Simulator Siemens Somatom Definition As with 3 mm slices from the vertex to the emerging aorta cross.

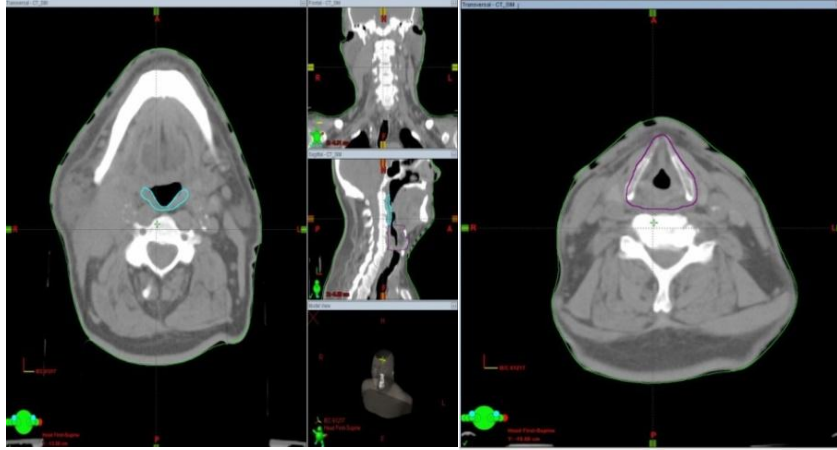


Fig. 1 – Upper pharyngeal constrictor (left) and supraglottic larynx (right) contoured as OAR.

The treatment plan was performed using Eclipse™ Treatment Planning System (Fig. 2) based on the CT simulation images. Image fusion and rigid registration with diagnostic i.v. contrast CT/MRI scan for a more precise target volume delimitation. Irradiation was performed in 3 sequential phases up to a maximum dose of 70Gy/35 fractions on the macroscopic volume of the primary tumor. High risk lymph nodes areas and macroscopically involved nodes received the maximum total dose of 66Gy/33 fractions, and the low-risk nodes levels were prophylactically irradiated with a total dose of 50Gy/25 fractions.

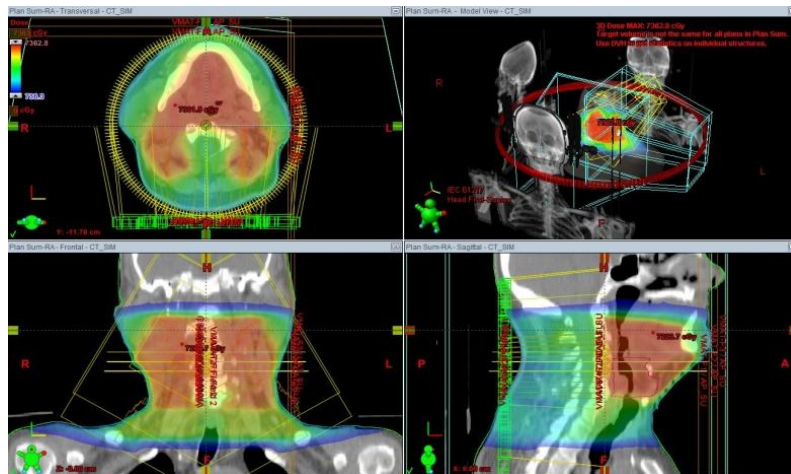


Fig. 2 – Dose distribution - “colorwash” representation in radiotherapy in VMAT for a case of neoplasm of oropharynx.

The treatment plans were done using RapidArc with single arc and implemented on the Varian Clinac iX linear accelerator, after being verified on ArcCHECK® phantom.

Christianen equation for NTCP values was used. A JAVA application has been created with a friendly interface (depicted in Fig. 3) that provides the NTCP value by introducing Dmean for supraglottic larynx and superior pharyngeal constrictor.

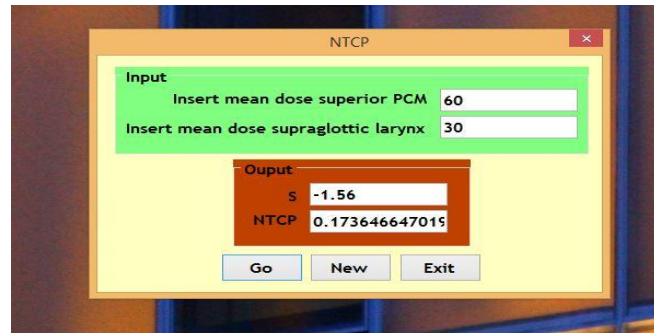


Fig. 3 – The graphical interface of the application that calculates NTCP with endpoint dysphagia.

3. Results and Discussion

Introducing Dmean obtained from the TPS in the computer application, NTCP values were generated.

Table 1
Dmean Values for the Superior Pharyngeal Constrictor and the Supraglottic Larynx; NTCP Calculated Values

	Case 1		Case2		Case3	
	Dmean (cGy)	NTCP (%)	Dmean (cGy)	NTCP (%)	Dmean (cGy)	NTCP (%)
superior pharyngeal constrictor	6907.4	47	6971.5	56.62	6443.9	53.75
supraglottic larynx	5547.1		5289.4		6940.3	

The most common late complications that affect the quality of life of radio-treated patients for head and neck cancers are dysphagia and xerostomia. Considering the complexity of structures involved in swallowing, it is difficult to assess the contribution of each of them to the occurrence of dysphagia (Narayanasamy *et al.*, 2015).

Lyman normal tissue complication probability (NTCP) model is based on DVH of the OARs.

Luxton *et al.* presented the values of the main parameters of the model: TD50/5, slope parameter (m), and the volume parameter (n) (Luxton *et al.*, 2008).

The study of Christianen includes 238 head and neck cancer patients treated with radiotherapy or chemo-radiotherapy. It appears that severe persistent and progressive swallowing dysfunction is associated with high doses received by the structures of upper pharyngeal region. Severe dysphagia is defined as swallowing dysfunction of grade 2 or higher at 6 months after RT or CH-RT which remained up to two year after the treatment. For long-term follow up, the importance of the dose to the supraglottic larynx appears to decline, while the effect of the dose to the superior PCM remains stable. The authors suggests that swallowing dysfunction can be prevented by maintaining the dose to the superior PCM as low as possible (Christianen, 2015).

On prospective cohort of 124 survivors included in the artscan study, Söderström and collaborators have tried to identify the dosimetric predictors of late dysphagia and the effect of elective lymph node irradiation. The main aim of the study was to identify in a multivariate ntcp model the prognostic factors of late dysphagia. They found that the mean dose to the superior pharyngeal constrictor and swallowing complaints at baseline were associated to patient reported choking and dose to the middle pharyngeal constrictor and post-radiotherapy neck dissection were predictors for late dysphagia (Söderström *et al.*, 2017).

From a dosimetric point of view the sparing of glottic larynx, oral cavity and superior pharyngeal constrictor is associated with preserved long-term swallowing function. These constraints are currently undergoing prospective validation. Beam-split IMRT techniques offer protection of the glottic larynx reducing the risk of aspiration. Dosimetric constraints: $V_{30} < 65\%$ and $V_{35} < 35\%$ for anterior oral cavity and $V_{55} < 80\%$ and $V_{65} < 30\%$ for high superior pharyngeal constrictors have been associated with a decrease in the risk of severe dysphagia (Schwartz *et al.*, 2010).

4. Conclusions

Radiobiological models - used more and more frequently as a predictor of toxicity and tumor control in IMRT and VMAT radiotherapy. The NTCP model for dysphagia can help the clinician to guide the post-radiotherapy supportive care treatment in order to reduce the effects of severe dysphagia and to prevent its complications. The application provides user friendly and easy calculation using a complex mathematical equation.

REFERENCES

- Christianen M.E., Verdonck-de Leeuw I.M., Doornaert P. *et al.*, *Patterns of Long-Term Swallowing Dysfunction after Definitive Radiotherapy or Chemoradiation*, *Radiother. Oncol.*, Oct., **117**, 1, 139-144 (2015).
- Denaro N., Merlano M.C., Russi E.G., *Dysphagia in Head and Neck Cancer Patients: Pretreatment Evaluation, Predictive Factors, and Assessment during Radio-Chemotherapy, Recommendations.*, *Clin. Exp. Otorhinolaryngol.*, Sep., **6**, 3, 117-126 (2013).
- Luxton G., Keall P.J., King C.R., *A New Formula for Normal Tissue Complication Probability (NTCP) as a Function of Equivalent Uniform Dose (EUD)*, *Phys. Med. Biol.*, **53**, 23-36 (2008).
- Narayanasamy G., Pyakuryal A.P., Pandit S., Vincent J., Lee C., Mavroidis P., Papanikolaou N., Kudrimoti M., Sio T.T., *Radiobiological Evaluation of Intensity Modulated Radiation Therapy Treatments of Patients with Head and Neck Cancer: A Dual-Institutional Study*, *J. Med. Phys.*, **40**, 165-169 (2015).
- Roe J.W., Drinnan M.J., Carding P.N. *et al.*, *Patient-Reported Outcomes Following Parotid-Sparing Intensity-Modulated Radiotherapy for Head and Neck Cancer. How Important is Dysphagia?* *Oral Oncol.*, Dec., **50**, 12, 1182-1187 (2014).
- Schwartz D.L., Hutcheson K., Barringer D. *et al.*, *Candidate Dosimetric Predictors of Long-Term Swallowing Dysfunction after Oropharyngeal Intensity-Modulated Radiotherapy*, *Int. J. Radiat. Oncol. Biol. Phys.*, Dec. 1, 78, 5, 1356-1365 (2010).
- Söderström K., Nilsson P., Laurell G. *et al.*, *Dysphagia - Results from Multivariable Predictive Modelling on Aspiration from a Subset of the ARTSCAN Trial*, *Radiother. Oncol.*, Feb., **122**, 2, 192-199 (2017).

O APLICAȚIE PE CALCULATOR PENTRU
PREDICȚIA RISCULUI DE DISFAGIE ÎN RADIOTERAPIA CANCERULUI
CAPULUI ȘI GĂTULUI

(Rezumat)

Disfagia este o complicație severă tardivă în radioterapia cancerului capului și gâtului. Riscul asociat aspirației, pierderea în greutate și afectarea calității vieții sunt doar câteva dintre consecințe. Limitarea dozei la nivelul mușchilor constrictori faringieni și a laringelui, scade riscul de disfagie tardivă pentru pacienții iradiați pentru cancer de cap și gât local avansat

Modelul radiobiologic propus de Christianen și colab. pentru evaluarea disfagiei tardive poate oferi un prognostic bun prin calcularea valorilor NTCP (probabilitatea de complicație a țesutului normal) utilizând doza mediană primită de laringele supraglotic și constrictorul faringian superior, conturați ca OAR (organe cu risc). Am proiectat o aplicație simplă Microsoft Windows pentru calculul simplu al riscului de disfagie post-radioterapie în neoplasmale capului și gâtului.

BULETINUL INSTITUTULUI POLITEHNIC DIN IAȘI
Publicat de
Universitatea Tehnică „Gheorghe Asachi” din Iași
Volumul 63 (67), Numărul 3, 2017
Secția
MATEMATICĂ. MECANICĂ TEORETICĂ. FIZICĂ

DOSIMETRIC COMPARISON BETWEEN IMRT AND 3D-CRT TECHNIQUES IN POSTSURGICAL RADIOTHERAPY OF A PLEOMORF LIPOSARCOMA OF THE THIGH

BY

OVIDIU NICOLAE PĂGUȚE¹, CAMIL CIPRIAN MIREȘTEAN¹,
CĂLIN GHEORGHE BUZEA^{1,*}, RALUCA APOSTU¹, SIMONA CÎRDEI¹,
TUDOR CIOBANU¹, COSMIN SAFTA¹ and DRAGOȘ TEODOR IANCU^{1,2}

¹Regional Institute of Oncology Iași

²“Grigore T. Popa” University of Medicine and Pharmacy, Iași,

Received: October 23, 2017

Accepted for publication: November 27, 2017

Abstract. Pleomorphic liposarcoma represents approximately 5% to 15% of all liposarcomas and it is much more aggressive than other liposarcoma subtypes and highly resistant to conventional treatment. Radiotherapy was associated with improved overall survival compared with surgery alone. We present the case of a 74-year-old patient, diagnosed with pleomorphic liposarcoma, who after complete healing from surgery, was guided to the radiotherapy department where he received postoperative radiotherapy at a total dose of 66Gy/33fr. The technique chosen was intensity-modulated radiotherapy, after a dosimetric comparison between intensity-modulated radiotherapy and three-dimensional conformal radiation therapy techniques was performed on the same tumor volume. The use of new radiation techniques, like intensity-modulated radiotherapy has improved quality of life and dose localizations, increasing local control and disease-free survival and at the same time a decrease in early and late effects of radiotherapy including bone fractures, oedema and joint stiffness.

Keywords: pleomorphic liposarcoma; radiotherapy; intensity-modulated radiotherapy; three-dimensional conformal radiation therapy; dosimetry.

*Corresponding author; *e-mail*: calinb2003@yahoo.com

1. Introduction

Liposarcoma (LPS) is the most common soft tissue sarcoma (STS) (Nassif *et al.*, 2016), accounting for approximately 20% to 25% of all STS (Hui, 2016). Pleomorphic liposarcoma (PLS) represents approximately 5% to 15% of all liposarcomas and it is much more aggressive than other LPS subtypes and highly resistant to conventional treatment (Peng *et al.*, 2017). PLS is a clinically, histologically and cytogenetically distinct form of liposarcoma and is the rarest subtype, it can occur in lower limbs, mediastinum, liver, orbit, paratesticular region and also as a pure dermal tumor (Bathla *et al.*, 2013).

Complete surgical resection is the main local disease treatment method. Radiotherapy (RT) and conventional cytotoxic chemotherapy remain controversial for metastatic or unresectable LPS (Peng *et al.*, 2017).

Radiotherapy was associated with improved overall survival compared with surgery alone when delivered as either preoperative radiotherapy or postoperative radiotherapy (Nussbaum *et al.*, 2016).

2. Case Report

We present the case of a 74 year-old patient with multiple cardiovascular pathological antecedents who presented herself in the surgery service in June 2015, claiming the appearance of a tumor on the anterior-medial face of the right thigh, declaring an evolution of about 7 months.

After performing an ultrasound guided puncture, whose anatomico-pathological outcome confirmed the presence of a sarcoma like tumor, the patient underwent an MRI examination. The exam highlighted a large 131/66/71 mm tumor formation in contact with the cortical bone encompassing the femoral vasculo-nerve package on the right thigh. Subsequently, she underwent surgery for excision of the tumor.

The anatomico-pathological outcome confirmed the presence of a pleomorphic grade II liposarcoma (FNCLCC) pT2bNx-G2, R1 resection. After complete healing, the patient was guided to the radiotherapy department where he received postoperative radiotherapy at a total dose of 66Gy/33fr.

The technique chosen was intensity-modulated RT (IMRT), after a dosimetric comparison between IMRT and three-dimensional conformal radiation therapy (3D CRT) techniques was performed on the same tumor volume.

3. Materials and Methods

The patient was simulated with CT-Simulator Siemens Somatom Definition AS, lower extremities protocol, 3 mm slices thickness, in the dorsal decubitus position, and the isocentre was established at the pelvic level (the anatomical projection of the great left and right trochanter and pubic

symphysis). We also fixed a metal wire on the postoperative scar. The treatment plan was performed in Eclipse 11 Treatment Planning. After performing a fusion between preoperative diagnostic images and those obtained at simulation, the gross tumor volume (GTV) preoperative volume was outlined. The clinical target volume 66 (CTV66) should encompass the entire GTV preoperative and immediate area of surgical disruption + 1 to 2 cm margin in the longitudinal plane + 1.5 cm margin in the transverse plane. This may, but not always, include all surgically disturbed tissues, scars, and drain sites, which may be included in a wider subclinical elective volume (Nancy *et al.*, 2015). To create the planning target volume (PTV) we expanded the CTV66 by adding +0.5 cm margin.

The outlined risk organs were: left and right femoral head, bladder, rectum, vagina, left and right labia, according to RTOG (Fig. 1).



Fig. 1 – The contoured OAR and PTV.

In the thigh sarcoma RT, vulva (vagina + labia) is not defined as a OAR, but its contouring and dosimetric constraints application can reduce the risk of overdosage by inverse planning when treatment planning systems (TPS) randomly chooses beam orientation. Studies on gynecological cancers have shown the risk of vaginal stenosis with implications for quality of life in radio-treated patients with external beam irradiation followed by brachytherapy (Morris *et al.*, 2017).

Daily kilovoltage image-guidance (Kv) was used in checking the position of the patient. The treatment was carried out with Varian Clinac iX 10MV.

4. Results

For a dosimetric observation, two treatment plans were created on the PTV volume: IMRT and 3D-CRT (Fig. 2).

After analyzing the dose-volume histogram (DVH), we obtained radiation dose data received by the organs at risk throughout the two techniques. Through the 3D-CRT technique, we obtained these values: vagina maximum dose 12.94Gy mean dose 6.686Gy, left labia maximum dose 16.90Gy mean

dose 12.01Gy, right labia maximum dose 39.73Gy mean dose 15.68Gy, right femoral head maximum dose 63.44Gy mean dose 18.85Gy, left femoral head maximum dose 6.68Gy mean dose 3.39Gy. And through IMRT technique, we obtained these values: vagina maximum dose 10.49Gy mean dose 2.47Gy, left labia maximum dose 9.92Gy mean dose 7.87Gy, right labia maximum dose 19.18Gy mean dose 10.89Gy, right femoral head maximum dose 66.49Gy mean dose 9.81Gy, left femoral head maximum dose 4.72Gy mean dose 1.53Gy. The conformity index (CI) for 3D-CRT was 1.1 and for IMRT 0.6.

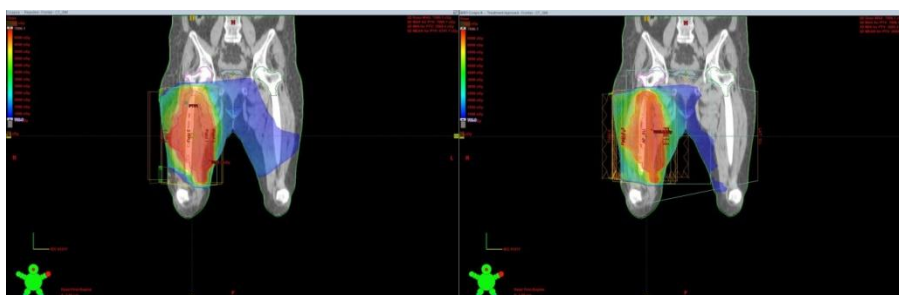


Fig. 2 – Color wash dose-volume histogram comparison between 3D-CRT(left) and IMRT (right).

5. Discussions

Adjuvant radiation therapy has been demonstrated to provide improved local control (LC) for STS of the extremity following limb-sparing surgery, and may be administered via brachytherapy or external-beam RT (EBRT). Many EBRT options exist, including conventional EBRT, IMRT and other advanced techniques including proton therapy (Folkert *et al.*, 2014). Dose conformity is especially important for large tumors such as sarcoma, providing adequate coverage of the periphery, and homogeneous coverage ensures that all tumor cells within the clinical volume receive adequate doses (Folkert *et al.*, 2014).

The use of new radiation techniques, like IMRT has improved quality of life (QOL) and dose localizations, increasing local control and disease-free survival and at the same time a decrease in early and late effects of RT including bone fractures, oedema and joint stiffness (Hoefkens *et al.*, 2016). Definitive radiotherapy for STS should be considered in clinical situations where no acceptable surgical option is available. Higher radiation doses yield superior tumor control and survival but, should be taken into account the complications that can occur in patients who receive doses over 68Gy (Kepka *et al.*, 2005).

CI is also an appropriate tool in treatment plan analysis in 3D CRT and IMRT. The CI defined as following:

$$CI = \frac{V95\%}{Volume\ of\ PTV}$$

V95% is the volume of PTV covered by at least 95% of prescribed dose (Salimi *et al.*, 2017).

The conformity index is a complementary tool that attributes a score to a treatment plan or that can compare several treatment plans for the same patient (Feuvret *et al.*, 2006).

Dose conformity is important for large tumors such as sarcoma, providing adequate coverage of the periphery, and homogeneous coverage ensures that all tumor cells within the clinical volume receive the prescribed doses (Folkert *et al.*, 2014).

The advantages of IMRT technique over 3D CRT and conventional techniques are reaching to the optimal dose distribution inside the tumor volume and decreasing the received dose by healthy tissues, these translate into improved outcomes and reduced toxicity (Feuvret *et al.*, 2006).

In theory the advantages of IMRT over non-IMRT are well accepted but insufficient evidence is available to conclude for the clinical setting. The main argument to choose IMRT over non-IMRT is its capacity to reduce toxicity. Results regarding survival, tumor control or other indexes of treatment efficacy remain generally inconclusive. Comparative case series show no differences in disease control and survival, unless dose escalation was used. The use of RT biologically “sterilizes” microscopic extensions of tumor, this limiting the need for wide resection margins, and allowing sparing of critical organs or neurovascular bundles. Another possibly favorable aspect of preoperative RT is the potential reduction of the seeding of microscopic sarcomatous cells at the time of surgical resection in addition to tumor shrinkage itself, which will greatly enhance the ability of the surgeon to achieve negative margins (Hoefkens *et al.*, 2016).

6. Conclusions

Pre- or postoperative Radiotherapy for STS of the extremity ensure excellent local control with acceptable treatment-related side effects but no statistically significant improvements in overall survival.

In the case presented above, we chose the IMRT irradiation technique even if in this case the CI was lower than the 3D-CRT techniques, in the desire to protect the OAR and another argument was the older age of the patient.

Also the percentage of volume receiving > 10Gy by the contralateral leg was lower by IMRT than 3D-CRT, reducing the risk of side effects or radiotherapy induced neoplasia.

REFERENCES

- Bathla V. *et al.*, *Giant Gluteal Pleomorphic Liposarcoma – A Rarity, Case Report*, GMJ, **68**, 2, 115-117 (2013).
- Feuvret L. *et al.*, *Conformity Index: A Review*, International Journal of Radiation Oncology, **64**, 2, 333-342 (2006).
- Folkert M.R. *et al.*, *Comparison of Local Recurrence with Conventional and Intensity-Modulated Radiation Therapy for Primary Soft-Tissue Sarcomas of the Extremity*, Journal of Clinical Oncology, **32**, 29, 3236-3242 (2014).
- Hoefkens F. *et al.*, *Soft Tissue Sarcoma of the Extremities: Pending Questions on Surgery and Radiotherapy*, Radiation Oncology, **11**, 136 (2016).
- Hui Jane Y.C., *Epidemiology and Etiology of Sarcomas*, Surg. Clin. N. Am., **96**, 901-914 (2016).
- Kepka L. *et al.*, *Results of Radiation Therapy for Unresected Soft-Tissue Sarcomas*, International Journal of Radiation Oncology, **63**, 3, 852-859 (2005).
- Morris L. *et al.*, *Radiation-Induced Vaginal Stenosis: Current Perspectives*, Int. J. Womens Health, **9**, 273-279 (2017).
- Nancy Y. Lee *et al.*, *Target Volume Delineation for 3D and IMRT*, X, 522 (2015).
- Nassif N.A. *et al.*, *Recent Advances in the Management of Liposarcoma*, F1000 Research (2016).
- Nussbaum D.P. *et al.*, *Preoperative or Postoperative Radiotherapy versus Surgery Alone for Retroperitoneal Sarcoma: A Case-Control, Propensity Score-Matched Analysis of a Nationwide Clinical Oncology Database*, The Lancet, **17**, 7, 966-975 (2016).
- Peng Y. *et al.*, *Effective Apatinib Treatment of Pleomorphic Liposarcoma: A Case Report*, Medicine, **96**, 33, 7771 (2017).
- Salimi M. *et al.*, *Assessment and Comparison of Homogeneity and Conformity Indexes in Step-and-Shoot and Compensator-Based Intensity Modulated Radiation Therapy (IMRT) and Three-Dimensional Conformal Radiation Therapy (3D CRT) in Prostate Cancer*, Journal of Medical Signals and Sensors, **7**, 2, 102-107 (2017).

COMPARAȚIE DOZIMETRICĂ ÎNTRE TEHNICILE IMRT ȘI 3D-CRT ÎN
RADIOTERAPIA POSTURGICALĂ A
LIPOSARCOMULUI PLEOMORF DE COAPSĂ

(Rezumat)

Liposarcomul pleomorf reprezintă aproximativ 5% până la 15% din toate liposarcoamele și este mult mai agresiv decât alte subtipuri de liposarcom și este foarte rezistent la tratamentul convențional. Radioterapia a fost asociată cu o supraviețuire globală îmbunătățită comparativ cu intervenția chirurgicală singură. Prezentăm cazul unei paciente în vârstă de 74 de ani, diagnosticată cu liposarcom pleomorf, care, după o vindecarea completă după intervenția chirurgicală, a fost direcționată către

departamentul de radioterapie, unde a beneficiat de radioterapie externă postoperatorie în doză totală de 66Gy/33fr. Tehnica aleasă a fost radioterapia cu intensitate modulată, după ce a fost efectuată o comparație dozimetrică între tehnica cu intensitate modulată și tehnica tridimensională conformațională pe același volum tumoral. Utilizarea de noi tehnici de radiație, cum ar fi radioterapia cu intensitate modulată, a îmbunătățit calitatea vieții, a crescut controlul local și supraviețuirea fără progresia bolii și în același timp, o scădere a efectelor acute și tardive ale radioterapiei incluzând fracturile osoase, edemul și rigiditatea articulară.

BULETINUL INSTITUTULUI POLITEHNIC DIN IAȘI
Publicat de
Universitatea Tehnică „Gheorghe Asachi” din Iași
Volumul 63 (67), Numărul 3, 2017
Secția
MATEMATICĂ. MECANICĂ TEORETICĂ. FIZICĂ

**THE INFLUENCE OF RADIOBIOLOGICAL MODELS IN
EVALUATION OF A TREATMENT PLAN REGARDING THE
RISK OF TOXICITY OF NEURAL STRUCTURES IN A PATIENT
WITH GLIOBLASTOMA TREATED WITH RADIOTHERAPY**

BY

**IUSTINA HĂTESCU¹, CĂLIN GHEORGHE BUZEA^{2,*}, CĂTĂLIN BORCIA¹
and DRAGOȘ TEODOR IANCU^{2,3}**

¹“Alexandru Ioan Cuza” University of Iași

²Regional Institute of Oncology, Iași

³“Grigore T. Popa” University of Medicine and Pharmacy, Iași

Received: October 23, 2017

Accepted for publication: November 27, 2017

Abstract. For a patient with fronto-parietal glioblastoma treated with radiotherapy, four different treatment plans, two with IMRT and two with 3D-CRT, have been analyzed.

All treatment plans were compared based on dose-volume histograms, coverage of the target volume and dose received by the OARs in order to establish which one had the best results.

We observed that one of the 3D-CRT plans was approved based on the already mentioned standards, as the best option available. Once the normal tissue complication probability was calculated, we found that for some organs, the risk of toxicity, although the evaluation of dose volume histograms did not suggest an increased risk, was higher in the approved plan.

*Corresponding author; *e-mail*: calinb2003@yahoo.com

It is important to take into consideration the NTCP for a better review of the risks that are most likely to appear after a shorter or a longer period of time, which will affect the patients' quality of life.

Keywords: fronto-parietal glioblastoma; IMRT; 3D-CRT; risk of toxicity; NTCP.

1. Introduction

For oncologists, high-grade gliomas (HGGs) is a very frustrating topic, as no significant progress has been made since the addition of Temozolomide (TMZ) concomitant and adjuvant to radiotherapy (Dhermain, 2014).

Glioblastoma is the most aggressive and frequent brain glial tumor. Standard treatment consists of surgery followed by radiotherapy concomitant with Temozolomide. Using high doses (60Gy) and irradiating large volumes (with 2-2.5 cm margins) around porencephal cavity makes it even more difficult to protect the OARs, such as brainstem, optic chiasm and optic nerves.

Afterwards, the risk of neuropathy was calculated with the help of radiobiological models such as Lyman-Kutcher Burman and EUD.

2. Materials and Methods

For a 57-year-old patient diagnosed with left parieto-occipital glioblastoma, with oligodendroglial component, concomitant postoperative radiotherapy has been proposed. Four treatment plans were proposed, 2 obtained using a 3D conformational and 2 with IMRT technique.

The patient was planned for radiotherapy up to 60Gy along with concurrent Temozolomide (75 mg/m²). The patient was positioned with a thermoplastic immobilization mask system and 3 mm CT scans of the head were obtained.

The European Organization of Research and Treatment of Cancer (EORTC) recommended a single-phase of 30 fractions with 2Gy/fraction technique. The GTV was defined on preoperative CT/MRI as the region of enhancement (without edema) or the surgical tumor BED plus any residual enhancing tumor that is seen on the planning scan for surgical treated patients using image fusion and rigid registration algorithm between of pre- and postoperative MRI/CT (Fig. 1).

The Clinical Target Volume (CTV) was defined from the Gross Target Volume (GTV) adding an isotropic margin of 2 - 3 cm, but this margin can be reduced in anatomical regions where tumor dissemination is unlikely. The planning target volume (PTV) was created adding a 0.5 to 0.7 cm, depending on systematic and random errors in dose delivery (Dhermain, 2014).

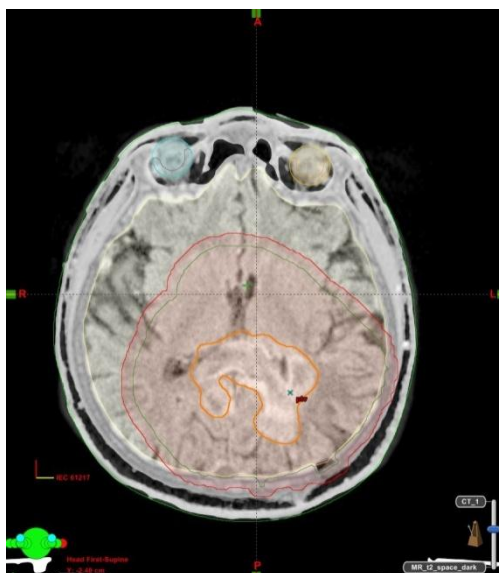


Fig. 1 – Image fusion and rigid registration between diagnostic MRI and CT simulation- target volume delineation.

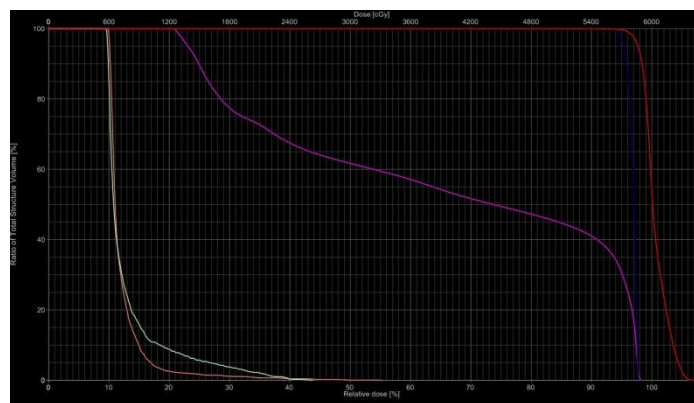


Fig. 2 – DVH curves for OARs (3D approved plan; light orange- left optic nerve, white- right optic nerve, purple- brainstem, blue- chiasm, red- PTV).

Following the treatment plan evaluation (coverage of the target volume, PTV, doses for OARs and dose-volume histograms) the treatment plan based on the 3D technique with a 6 MV beam was chosen (Fig. 2).

One of the plans prepared using the 3D-CRT technique, which was also among the approved ones, had the following characteristics: it was built on the 10 MV accelerator, the energy used was 6 MV, the total dose prescription was

60Gy delivered in 30 fractions with 2Gy/fraction. Five fields were used, the monitor units (MU) varied from 18 to 137, and 95% of PTV was covered by 97.68% of dose. The other 3D-CRT plan was completed on the 15 MV accelerator, the energy used was 6 MV and had the same fractionation. Five fields were used here also, MU varied from 18 to 136 and 95% of PTV was covered by 97.43% of dose. One of the plans made with the IMRT technique was delivered on the 10 MV accelerator, with a beam of 6 MV energy, same fractionation as the other two mentioned above. Here 7 fields were used, MU varied from 73 to 122 and 95% of the PTV was covered by 93.5% of dose. The other plan made by IMRT technique was made on the 10 MV accelerator, with a beam of energy of 6 MV, 9 fields were used this time, and 95% of the PTV was covered by 96% of dose (Fig. 3).

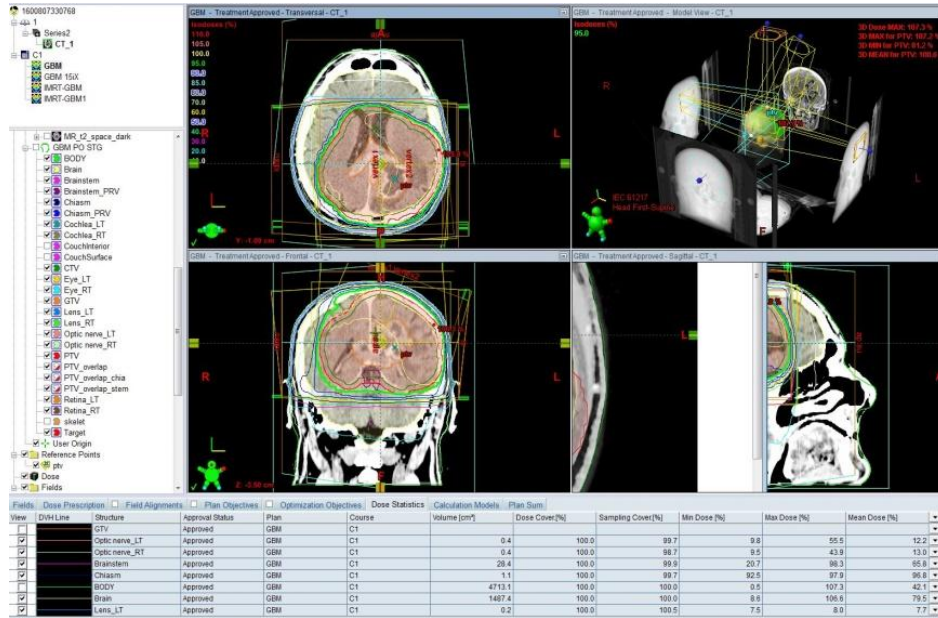


Fig. 3 – Glioblastoma 3D treatment plan (images from TPS eclipse).

Subsequently, the risk of neuropathy was calculated with the help of radiobiological models such as Lyman-Kutcher Burman (LKB) and EUD. One can use them to compute normal tissue complication probability (NTCP) and tumor control probability (TCP). The results are displayed in percents.

Parameters used for the LKB model are $TD50$, number of fractions, n , m , α/β and dose per fraction. The formula that describes the Lyman-Kutcher Burman model is

$$NTCP = \frac{1}{\sqrt{2\pi}} \int_{-\infty}^t e^{-\frac{x^2}{2}} dx \quad (1)$$

where

$$t = \frac{D_{ef} - TD_{50}}{mTD_{50}} \quad (2)$$

and

$$D_{ef} = (\sum_i v_i D_i^{1/n})^n \quad (3)$$

Parameter n determines the dose-volume dependence of a tissue and thus accounts for differences in tissue architecture; m controls the slope of the dose-response curve; TD_{50} represents the dose at which there is a 50% chance of complication, and thus dictates the position of the dose-response curve (Warkentin *et al.*, 2004). D_{ef} is the dose that, if distributed uniformly to the entire volume, will lead to the same NTCP as the real dose that unevenly distributed, and D_i is the dose given to a subvolume v_i .

The EUD model is described by the following formula:

$$NTCP = \frac{1}{1 + (\frac{TD_{50}}{EUD})^{4\gamma_{50}}} \quad (4)$$

where the equivalent uniform dose is

$$EUD = (\sum_i v_i D_i^a)^{\frac{1}{a}}. \quad (5)$$

EUD is defined as the equivalent biological dose that, when distributed uniformly, will lead to the same biological effect as the real one given by the unevenly distribution of the dose. Also, a and γ_{50} are dimensionless parameters, a having specific values for each tissue.

For the normal tissue complication probability (NTCP) evaluation RADBIOMOD was used, an application using Visual Basic for Applications (VBA) for Microsoft Excel. It includes multiple mathematical models for biological radiotherapy plan evaluation, a free, user-friendly program that offers similar results to other radiobiological modeling programs (Chang *et al.*, 2016).

For the evaluation, the DVHs for organs at risk are exported from the treatment planning program Eclipse, into ASCII format.

3. Results

The volumes in cmc of target volumes of the primary tumor (GTV, CTV and PTV) and D_{max} and D_{mean} for all treatments were compared (Figs. 4 and 5).

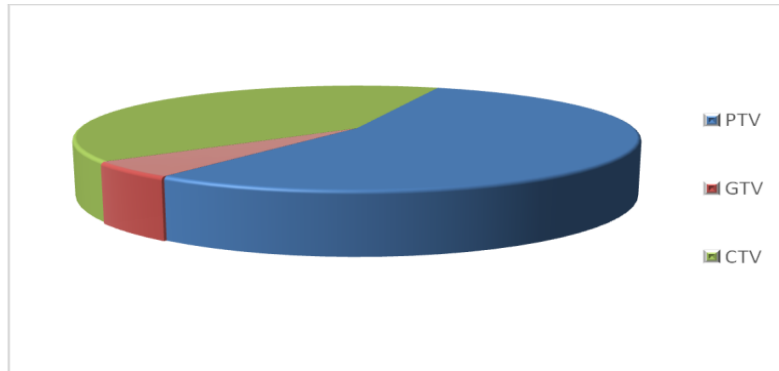


Fig. 4 – Graphic representation of Planning Target Volume (PTV), Gross Target Volume (GTV) and Clinical Target Volume (CTV).

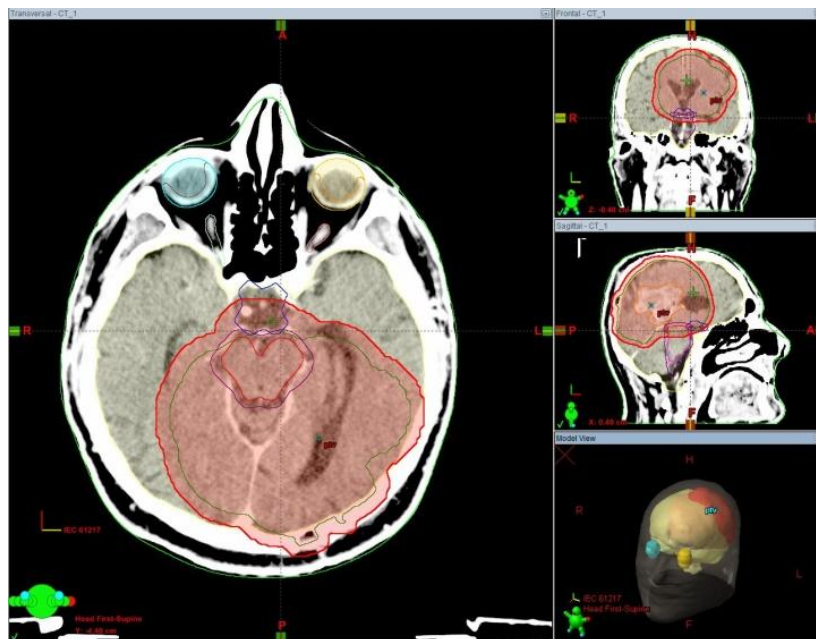


Fig. 5 – Target volumes and OARs for a glioblastoma radiotherapy plan.

For the brainstem, the maximum value of D_{\max} was obtained for the 3D approved plan, (59Gy) and the maximum dose of D_{mean} for brainstem was 39.49Gy for the 3D approved plan. For chiasm, the maximum value of D_{\max} was obtained for the 3D unapproved plan, 64.23Gy, and the maximum dose for D_{mean} was 58.1Gy, for the 3D approved plan (Figs. 6 and 7).

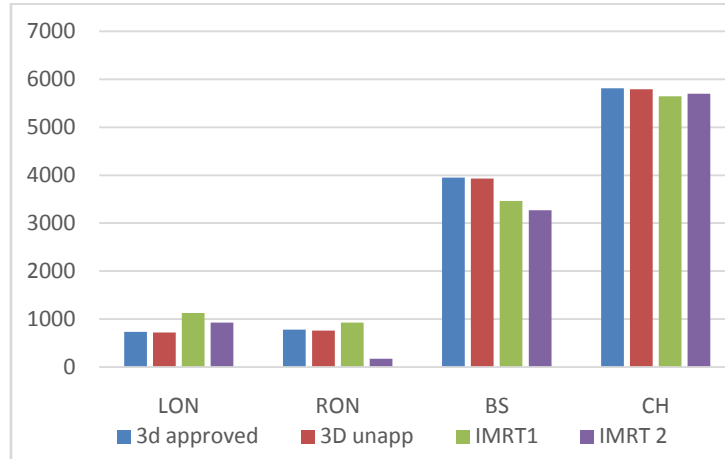


Fig. 6 – Graphic representation of Dmean for all 4 proposed plans (blue- 3D approved plan; red- 3D unapproved plan; green- IMRT1; purple- IMRT2).

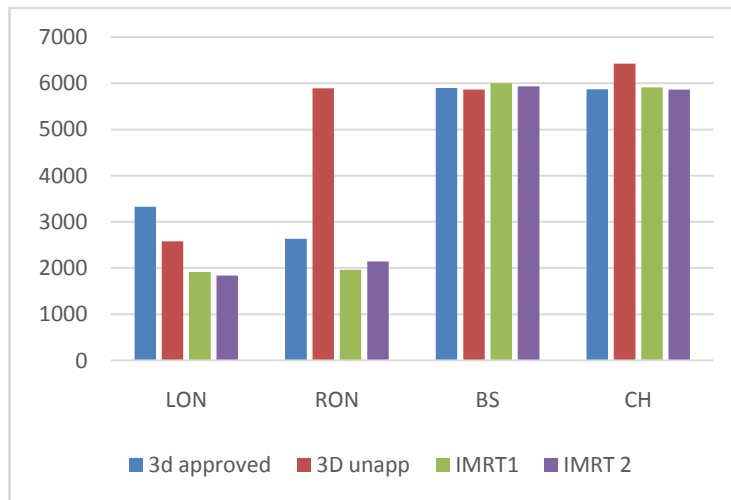


Fig. 7 – Graphic representation of Dmax for all 4 proposed plans (blue- 3D approved plan; red- 3D unapproved plan; green- IMRT1; purple- IMRT2).

NTCP values evaluated by the LKB model for left optic nerve were 0% for all 4 plans, and also the same for the right optic nerve. For brainstem NTCP was 0.49% for the approved 3D plan, 28.92% for the unapproved 3D plan, 0.82% for one IMRT plan (IMRT 1), and 0.37% for the other IMRT plan (IMRT 2). For the chiasm, values were: 2.92% for the 3D approved plan, 2.59% for the 3D unapproved plan, 1.84% for IMRT 1, and 2.1% for IMRT 2 (Fig. 8).

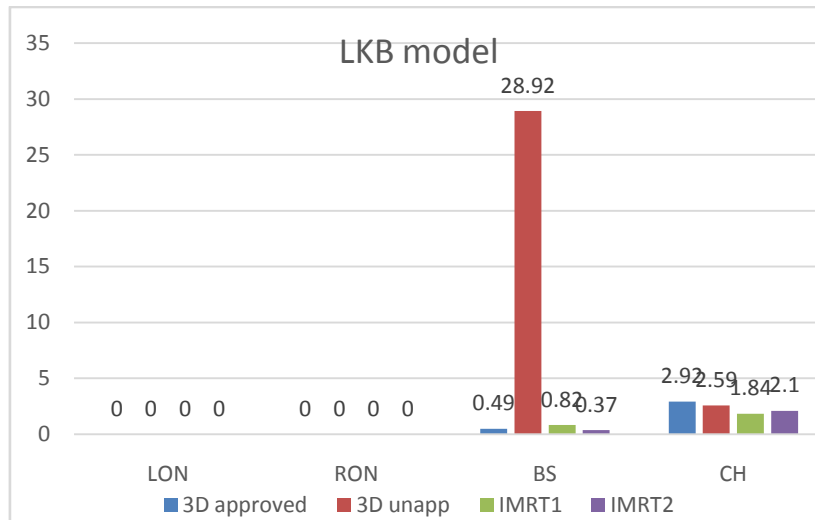


Fig. 8 – Graphic representation of LKB model values obtained for radiotherapy plans.

Different values were obtained when using EUD model. For the left and right optic nerve the values were equal to 0%. For brainstem, values were: 1.3% for the 3D approved plan, 22.49% for the 3D unapproved plan, 0.99% for IMRT 1 and 0.48% for IMRT 2. For chiasm we got 12.67% for the 3D approved plan, 11.93% for the unapproved 3D plan, 9.72% for IMRT 1 and 10.02% for IMRT 2 (Fig. 9).

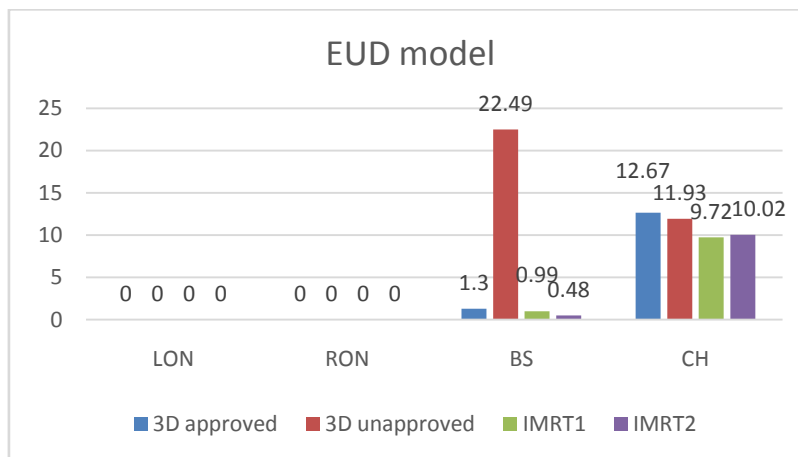


Fig. 9 – Graphic representation of EUD model values obtained for radiotherapy plans.

4. Discussions

In a cohort of 20 patients, Hermanto and coworkers demonstrated that IMRT maintained equivalent target coverage, and enabled dose reductions of neural structures: brainstem D_{mean} by 19.8% and D_{max} by 10.7%, optic chiasm D_{mean} by 25.3% and D_{max} by 22.6%, right optic nerve D_{mean} by 37.3% and D_{max} by 28.5%, and left optic nerve D_{mean} by 40.6% and D_{max} by 36.7% (Hermanto *et al.*, 2007).

Most of the studies have proved equivalence comparing 3D-CRT and IMRT for radiotherapy of glioblastoma in terms of target coverage, dose conformity and dose homogeneity (Wagner *et al.*, 2009).

The damage to optical structures can lead to optic neuropathy with potential of blindness, but toxicity to the brainstem can have fatal consequences. The entire brainstem may receive up to 54Gy using conventional fractionation with limited risk of severe or permanent neurological effects. Smaller volumes of the brainstem (1-10 mL) may tolerate a D_{max} of 59Gy for standard fractionation (Scocciati *et al.*, 2015).

A number of studies have been published which investigated the use of IMRT technique in glioblastoma treatment, but the results are hard to analyze because the heterogeneity of the cases included. Some patients were treated for recurrent diseases and only in some cases chemotherapy was administered. Aherne *et al.* observed a study including 31 patients treated with IMRT and 23 of them received chemo-irradiation with Temozolomide. The combination of IMRT at standard radiation doses with Temozolomide can lead to an increase in median overall survival. It may be possible that IMRT radiotherapy improves the quality of life of long-term surviving patients by reducing the dose to critical normal structures and normal brain tissue (Aherne *et al.*, 2014).

Few studies were reported on the comparison of clinical outcomes between IMRT and 3D-CRT in the treatment of high grade gliomas. A study including 54 patients try to determine whether IMRT improves clinical outcomes related to 3D-CRT for glioblastoma radiotreated patients. With no significant difference for toxicities between these techniques results suggested that IMRT is unlikely to improve local control and overall survival compared with 3D-CRT (Chen *et al.*, 2013).

5. Conclusions

A higher risk of brainstem toxicity corresponded to the approved plan, and a lower risk corresponded to an unapproved plan using the IMRT technique.

For minor differences between the values of D_{mean} and D_{max} , DVH and slide by slide evaluation of the dose curves, NTCP is a helpful tool for plan approval by the clinician.

In conclusion, even if the radiobiological models are not standard in the evaluation process of the treatment plan, under the circumstances of a complex dose distribution obtained through an IMRT technique, they can have a guiding role in therapeutic decision.

REFERENCES

- Aherne N.J., Benjamin L.C., Horsley P.J., *Improved Outcomes with Intensity Modulated Radiation Therapy Combined with Temozolomide for Newly Diagnosed Glioblastoma Multiforme*, *Neurol. Res. Int.*, 2014, 945620 (2014).
- Chang J.H., Gehrke C., Prabhakar R. *et al.*, *Radbiomod: A Simple Program for Utilizing Biological Modelling in Radiotherapy Plan Evaluation*, *Phys. Med. Jan.*, **32**, 1, 248-254 (2016).
- Chen Y.D., Feng J., Fang T., *Effect of Intensity-Modulated Radiotherapy versus Three-Dimensional Conformal Radiotherapy on Clinical Outcomes in Patients with Glioblastoma Multiforme*, *Chin. Med. J. (engl). Jun.*, **126**, 12, 2320-2324 (2013).
- Dhermain F., *Radiotherapy of High-Grade Gliomas: Current Standards and New Concepts, Innovations in Imaging and Radiotherapy, and New Therapeutic Approaches*, *Chin. J. Cancer. Jan.*, **33**, 1, 16-24 (2014).
- Hermanto U., Frija E.K., Lii M.J. *et al.*, *Intensity-Modulated Radiotherapy (IMRT) and Conventional Three-Dimensional Conformal Radiotherapy for High-Grade Gliomas: Does IMRT Increase the Integral Dose to Normal Brain?* *Int. J. Radiat. Oncol. Biol. Phys. Mar.* 15, **67**, 4, 1135-1144 (2007).
- Scoccianti S., Beatrice D., Gadda D. *et al.*, *Organs at Risk in the Brain and their Dose-Constraints in Adults and in Children: A Radiation Oncologist's Guide for Delineation in Everyday Practice*, *Radiotherapy and Oncology*, **114**, 230-238 (2015).
- Wagner D., Christiansen H., Wolff H., Vorwerk H., *Radiotherapy of Malignant Gliomas: Comparison of Volumetric Single Arc Technique (RapidArc), Dynamic Intensity Modulated Technique and 3D Conformal Technique*, *Radiother. Oncol.*, **93**, 593-396 (2009).
- Warkentin B., Stavrev P., Stravreva N. *et al.*, *A TCP-NTCP Estimation Module Using DVHs and Known Radiobiological Models and Parameter Sets*, *J. Appl. Clin. Med. Phys. Winter*, **5**, 1, 50-63 (2004).

INFLUENȚA MODELELOR RADIOBIOLOGICE ÎN EVALUAREA UNUI PLAN DE TRATAMENT PRIVIND RISCUL DE TOXICITATE A STRUCTURILOR NEURALE LA UN PACIENT CU GLIOBLASTOM TRATAT CU RADIOTERAPIE

(Rezumat)

Pentru un pacient cu glioblastom fronto-parietal radio-tratat, s-au analizat patru planuri diferite de tratament, două cu IMRT și două cu 3D-CRT.

Toate planurile de tratament au fost comparate pe baza histogramei doză-volum, acoperirea volumului țintă și a dozei primite de OAR pentru a stabili care dintre ele a avut cele mai bune rezultate.

Am observat că unul dintre planurile 3D-CRT a fost aprobat pe baza standardelor deja menționate, ca fiind cea mai bună opțiune disponibilă. Odată ce probabilitatea de complicații a țesutului normal a fost calculată, am constatat că, pentru unele organe, riscul de toxicitate, deși evaluarea histogramei volumului dozei nu a sugerat un risc crescut, a fost mai mare în cazul planului aprobat.

Este important să se țină seama de NTCP pentru o mai bună revizuire a riscurilor, care sunt cel mai probabil să apară după o perioadă mai scurtă sau mai lungă, ceea ce ar afecta calitatea vieții pacienților.

